# Design of a Single-Degree-of-Freedom Exoskeleton for Thumb Rehabilitation in Conjunction with FINGER

A Thesis

Presented in Partial Fulfillment of the Requirements for the

Degree of Master of Science

with a

Major in Mechanical Engineering

in the

College of Graduate Studies

University of Idaho

by

Kyle J. Morse

Major Professor: Eric T. Wolbrecht, Ph.D.

Committee Members: Joel C. Perry, Ph.D.; Matthew E. Riley, Ph.D.

Department Administrator: Steven W. Beyerlein, Ph.D.

June 2015

# Authorization to Submit Thesis

This thesis of Kyle Morse, submitted for the degree of Master of Science with a major in Mechanical Engineering and titled “Design of a Single-Degree-of-Freedom Exoskeleton for Thumb Rehabilitation in Conjunction with FINGER," has been reviewed in final form. Permission, as indicated by the signatures and dates below, is now granted to submit final copies to the College of Graduate Studies for approval.

Major Professor: _____ Date: _____
Eric T. Wolbrecht, Ph.D.

Committee Members: _____ Date: _____
Joel C. Perry, Ph.D.

_____ Date: _____
Matthew E. Riley, Ph.D.

Department Administrator: _____ Date: _____
Steven W. Beyerlein, Ph.D.

# Abstract

This thesis presents the development of an exoskeleton for post-stroke thumb rehabilitation. This exoskeleton is a six-bar planar single-degree-of-freedom mechanism that controls the position and angle of the middle phalanx of the thumb. It is an add-on for the finger rehabilitation device FINGER for grasp training, which is a fundamental activity of daily living.

The trajectory of the middle phalanx of a healthy human thumb was characterized with color-marker based motion tracking. Mechanisms were synthesized by minimizing the error between the end-effector of the mechanism solutions and the trajectory of the thumb. A mechanism solution was selected for design based on its manufacturability and mechanical advantage. Both the mechanism and an adjustable module to attach the mechanism to the housing for FINGER were designed, then manufactured using a combination of additive manufacturing and CNC machining. This provided a prototype for evaluation to inform future design efforts.

# Acknowledgments

It is my sincere pleasure to acknowledge my family and friends without whose prayers and support I could not have completed this degree. I would also like to acknowledge the NASA Idaho Space Grant Consortium through which I was funded throughout my time at Idaho. I would finally like to acknowledge and thank Dr. Wolbrecht, my major professor, and Stephen Goodwin and Jeremiah Schroeder, my colleagues, for their hard work, input, and assistance on this project as well as Dr. Perry and Dr. Riley for their input on my committee.

The project described was supported by NIH-R01HD062744 from the National Center for Medical Rehabilitation Research at the National Institute of Child Health and Human Development, and the National Center for Research Resources and the National Center for Advancing Translational Sciences, National Institutes of Health, through Grant UL1 TR000153. The content is solely the responsibility of the authors and does not necessarily represent the official views of the NIH.

## Dedication

This thesis is dedicated to my grandfather, a Marine Corps fighter pilot, mechanical engineer, and follower of Christ.

# Table of Contents

# List of Figures

# List of Tables

# Chapter 1. Introduction

## 1.1 Background

Nearly 800,000 people suffer a stroke in the United States each year. It is estimated that through 2012, around 6.6 million Americans had suffered at least one stroke in their life. As stroke is a leading cause of long-term disability, these numbers point to a serious health problem that not only affects victims of stroke and their families, but leads to an estimated annual financial burden of $34 billion in the United States alone due to the combined costs of health care, lost productivity, etc. [1]

A common disability associated with stroke is hemiparesis of the upper limb. A pair of studies on stroke patients found that 70 to 76 percent of stroke survivors had upper-limb hemiparesis after the stroke [2]. Recovery of upper-limb dexterity was found to be poor with only 28 to 45 percent regaining some dexterity [3]. Depending on the study, a mere 11.6 to 13.6 percent of patients made a complete recovery from upper-limb impairment following a stroke [4].

## 1.2 Stroke Therapy

In an effort to enhance recovery from stroke for the millions of affected people, a significant amount of research has gone into determining optimal procedures for post-stroke rehabilitation. At its core, rehabilitation is a cyclical procedure of assessment, goal setting, and intervention [5]. The consensus among medical and research professionals regarding timing of therapy is that while a few days should be given to allow penumbral tissue to initiate healing after a stroke, waiting longer than a week to begin intensive therapy may be detrimental to recovery [6].This is because fewer days between the onset of the stroke and the start of rehabilitation is significantly associated with better functional outcomes [7]. No

cut-off time for therapy has been established as improvement of movement has been observed over six months following the onset of a stroke [8]. These findings point to the importance of available therapy options throughout a patient's recovery.

It is important to recognize the best practices for post-stroke therapy in order to maximize a patient's potential for recovery. A review of stroke therapy in [9] supported the concept that intensive, repetitive, task-specific interventions focused on activities of daily living were most effective for promoting motor recovery. Another review tempered this finding by noting that most of the effects of therapy were limited to trained functions and activities [10].

A variety of therapy methods have been evaluated for effectiveness beyond conventional therapy. These methods have been studied in conjunction with conventional rehabilitation and as the sole means of therapy. Simple methods such as constraint-induced movement therapy and mental practice have both demonstrated effectiveness [11-12]. More active means of therapy, such as electrostimulation of impaired musculature, have also been found to enhance upper extremity motor recovery. However, electrostimulation can be painful for the patient [13-14]. Supplying the patient with extra information via electromyographic biofeedback has not shown a significant positive effect [15].

## 1.3 Robot-Assisted Stroke therapy

Post-stroke movement training using robotic devices under the supervision of a trained therapist has also been an active area of research for therapeutic applications with patients who have suffered a stroke. Multiple reviews and meta-analyses of the literature have shown that robotic rehabilitation promotes gains similar to those seen with intensive conventional therapy with very rare adverse effects [16-18]. Some evidence suggests that

therapy with robotic devices may even outperform conventional therapy [19]. This difference is no longer significant when compared with intensive therapy. Yet, intensive therapy is far more expensive than robot-assisted therapy as one study found the per-patient cost to be $5,152 for robot-assisted therapy, while intensive therapy cost $7,382 [19]. Furthermore, there are not enough therapists to universally provide intensive therapy.

Robotic methods have a number of key advantages over conventional therapy. First, the repeatable movements of which robots are capable are perfectly suited to the intensive, repeatable interventions shown to be effective in the literature, without straining the administering therapist [20]. Robotic devices are also well-suited for quantifying the forces and movements associated with rehabilitation. These measurements can be used for targeted assessment to improve an individual patient's therapy [21]. Visual feedback based on the measured performance of the patient has also been shown to enhance motivation [22]. These measurements may also be used to expand the body of knowledge on stroke rehabilitation by improving the understanding of specific mechanisms of neuroplasticity supporting motor learning [23].

Beyond reducing physical strain on the therapists through semi-autonomous operation, robotic devices can also provide more finely tuned sensing and manipulation than a therapist can in certain situations [23]. This may permit the construction of novel methods of intervention. By having multiple robotic devices, therapists may also use the robots to leverage their time and better serve more patients [24].

## 1.4 Robotic Devices for Stroke Therapy

A review in [25] covers a wide range of robots that have been designed specifically for post-stroke rehabilitation of impaired upper limbs. The reviewers categorized the

mechanical design of the robotic devices by exoskeletons and end-effector devices. They noted that electric actuators or pneumatic-pressure systems are typically used to power these devices. They further classified the robots by target rehabilitation area. These areas included the arm, wrist, hand, fingers, or a combination of the upper limbs. Robotic devices for the rehabilitation of the hand and fingers have gloves included as a third category to end-effector and exoskeleton devices.

Glove robots (for example PneuGlove [26]) are donned over the hand as their name suggests. The close fit of a glove may enhance patient comfort. The low profile of the glove may also be advantageous for rehabilitation tasks in constrained spaces. Still, a glove may interfere with patient sensory feedback. Glove-based devices may also be difficult to put on for an impaired individual due to increased tone [27]. The flexible nature of the attachment of glove-based devices to the hand intuitively makes precise control more difficult.

End-effector robots (such as the device in [28]) usually attach to the most distal part of a subject's limb, simplifying the device's structure. However, this initial simplicity necessitates more complicated control algorithms for applications with multiple potential degrees-of-freedom, such as control of the hand [25]. This may increase the chance of injury during therapy. Like a glove, the inherent design of the interface between the robot and the hand has the potential to interfere with interventions that require patient sensory feedback.

Exoskeleton robots (like HEXORR [29]) typically interface with the dorsal side of the hand and fingers. Their structure imitates the skeletal structure of the limb permitting precise control since each limb segment is attached to a corresponding device segment. As with end-effector robots, the complexity of control significantly increases with higher degrees of freedom [25].

Rehabilitation robotic devices are typically powered using either electric actuators or pneumatic pressure. Electric actuators are more common, but a few systems (such as Pneu-WREX [30]) use pneumatic pressure due to its high strength-to-weight ratio. Still, the requirement of a compressor may make pneumatic actuation less convenient in some cases than electric actuators.

A problem with geared electric motors is that they may exhibit poor backdrivability. Backdrivability is the potential for a motor to easily be moved when it is turned off. This is advantageous in rehabilitation robots for both patient safety and comfort. This feature may also allow for the design of a controller that turns off the assistance of the actuator to prevent slacking by the patient. Linear electric motors, such as the ServoTube Actuator by Dunkermotoren Linear Systems, can provide backdrivability along with high speed and a large stroke when the design of the device permits their use.

Exoskeletons designed for rehabilitation of the hand such as HEXORR and HWARD [31] often are used to train grasping movements using both the fingers and thumb. Standalone devices for all [32] or some [33] of the fingers without a thumb and just a thumb [34-35] have also been developed. Because grasping is such an important activity of daily living, having a device that can control both the fingers and the thumb is ideal.

## 1.5 FINGER and Summary of Thumb Exoskeleton Project

At the University of Idaho, a robotic rehabilitation device named FINGER (Finger Individuating Grasp Exercise Robot) [33] has been developed together in collaboration with researchers at The University of California Irvine. This device is shown in Figure 1.

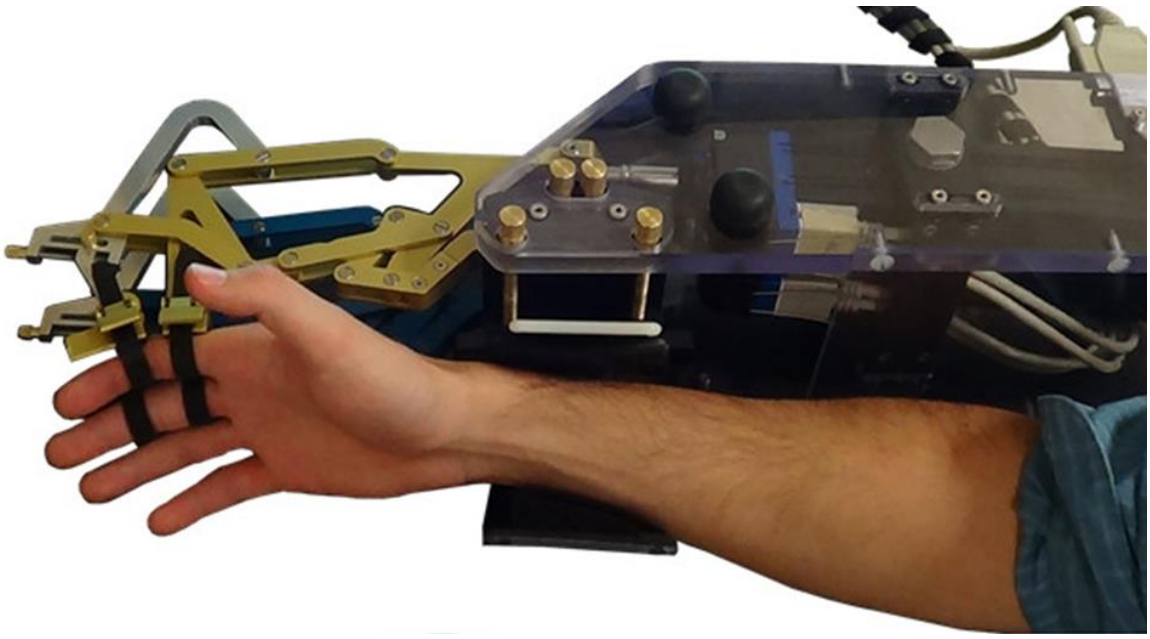

Figure 1. A picture of FINGER (Finger INdividuating Grasp Exercise Robot).

FINGER is capable of assisting stroke patients with precise movement of their index and middle fingers individually through a naturalistic curling motion. This movement is controlled by a pair of single-degree-of-freedom eight-bar mechanisms that contact the proximal and middle phalanges of the attached fingers. The distal phalanges are left open for tactile feedback during therapy. These mechanisms are independently driven by two brushless linear DC motors. The low friction and inertia of the mechanism and the linear motor combination creates a highly backdrivable system that can achieve high-bandwidth force control.

FINGER demonstrated its potential as a rehabilitation and research device in preliminary testing with moderately-impaired and severely-impaired individuals [33]. By developing a thumb exoskeleton to be added on to the FINGER robot, the capabilities of the device can be expanded. These additional capabilities may include full grasp training, the study of finger-thumb coupling, and other tasks. The work herein focuses on the design

process for developing a thumb mechanism add-on to FINGER and creating an initial prototype using that process.

The following chapters describe the design and development of the thumb exoskeleton mechanism including the following processes: characterization of the motion of the thumb with motion tracking; mechanism synthesis; and mechanical design and prototyping. Initially, the three-dimensional motion of the middle phalanx of the thumb is characterized using color-based motion tracking [36-37]. Next, the process of mechanism synthesis to design a linkage that follows the trajectory of the thumb is discussed. The selection of a mechanism from the potential solutions produced by mechanism synthesis was the next step. After that, designing a mechanism with a beneficial mechanical advantage profile from the solutions obtained during mechanism synthesis and the fabrication of an initial prototype is described. This thesis concludes with a discussion of the work completed and makes recommendations for future work.

# Chapter 2. Thumb Path Characterization

## 2.1 Introduction

This chapter discusses the motion tracking and data analysis used to determine the position and angle of the middle phalanx of the thumb during a tip pinch grasp [38]. The three-dimensional track of the thumb provided target points for the synthesis of the mechanism. The motion of tip pinch grasp was chosen as it appeared to be similar to the principal components of the postural synergies associated with hand use [39]. This should make it useful for training grasping. Additionally, the thumb motion complemented the naturalistic curling motion of the index and middle fingers controlled by the FINGER mechanism. This fit the goal of creating a thumb mechanism to work with FINGER.

## 2.2 Motion Tracking

Color-based motion tracking was used due to the small number of required markers and the simplicity of the method. Three colors were placed on a marker frame attached to the middle phalanx of the thumb with a hook and loop system as shown in Figure 2.

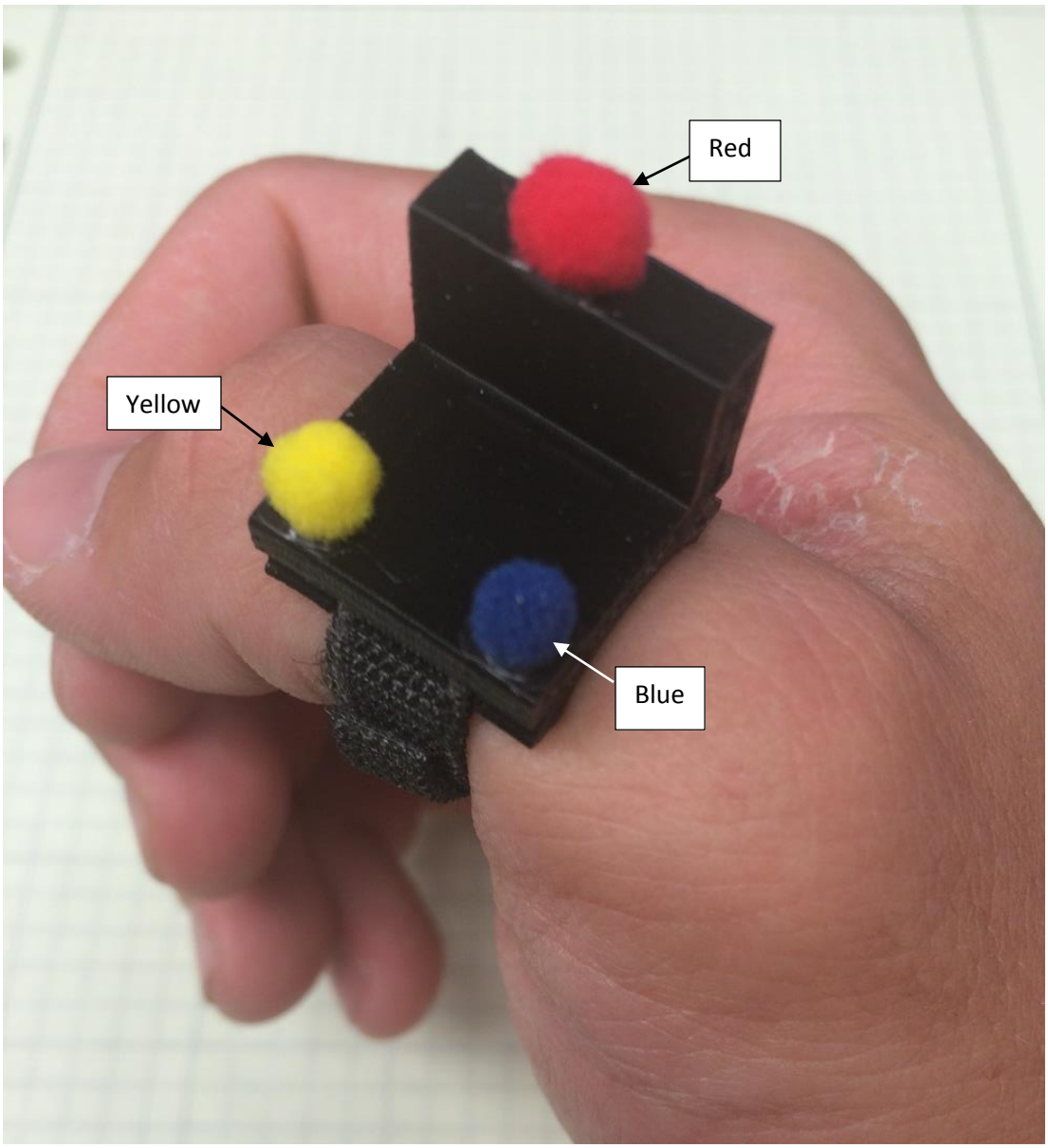


Figure 2. Marker frame attached to the thumb with red, yellow and blue markers.

The relative position of each marker was known. The red marker on the backside was also raised up a known distance to keep it in view of the side camera during the entire motion. The specific dimensions relating the markers to one another on the frame are shown in Figure 3.

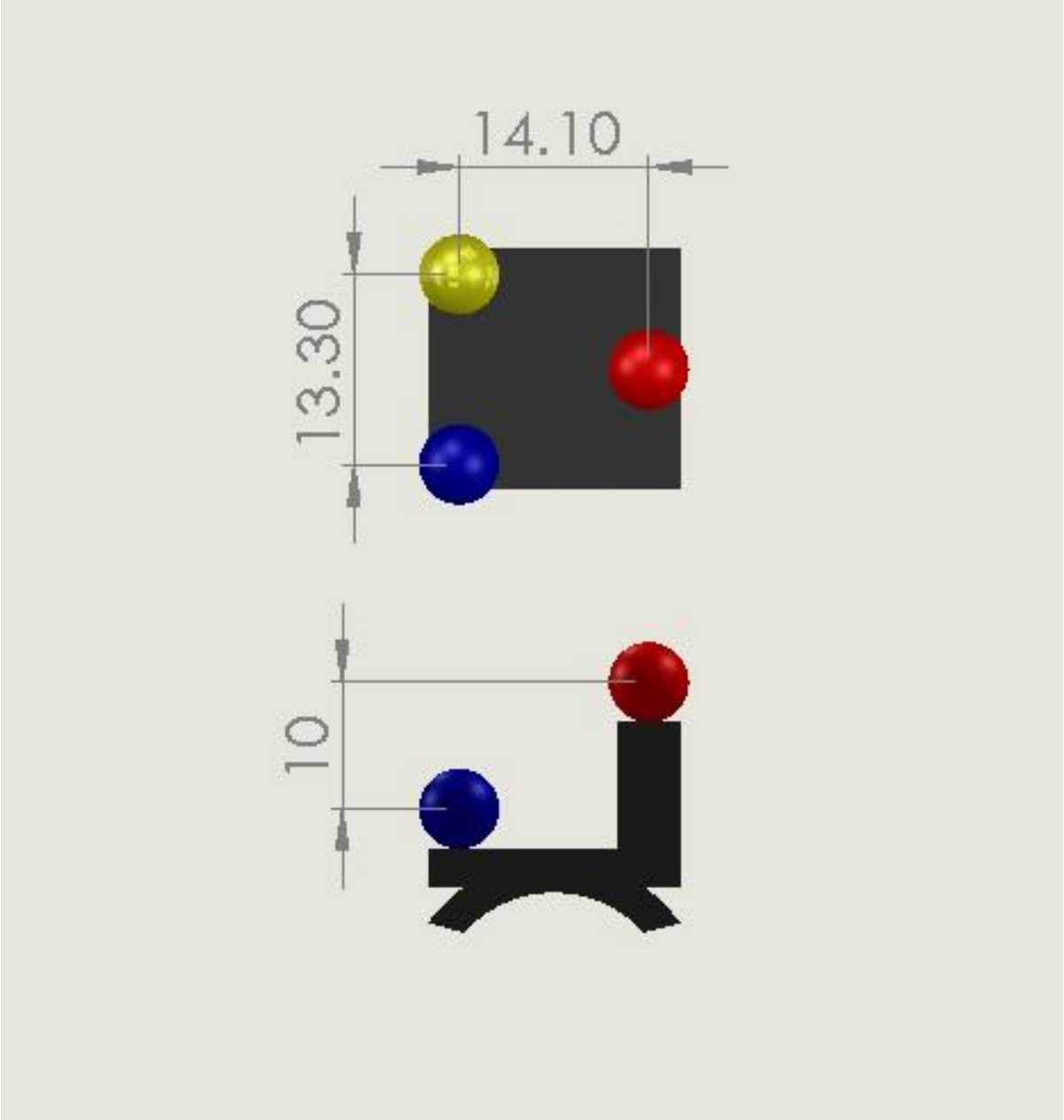


Figure 3. Marker frame top and side view with dimensions in millimeters.

Two cameras were used for the motion tracking to obtain three-dimensional information about the motion of the thumb. Each camera was placed an equal distance of 6.5 inches from the midpoint of the thumb's motion. The equal distance maintained the same scale for each camera to mitigate distortion when the two frames were combined to create the three-dimensional model of the thumb motion. The distance of 6.5 inches was chosen as it was the closest distance that both cameras could be to the thumb while each had a full view of the

markers during the full grasp motion. The apparatus used for motion tracking consisted of two cameras attached to an aluminum frame with a mock-up of FINGER positioned to put the thumb in the correct position under the cameras. The motion tracking apparatus is shown in Figure 4.

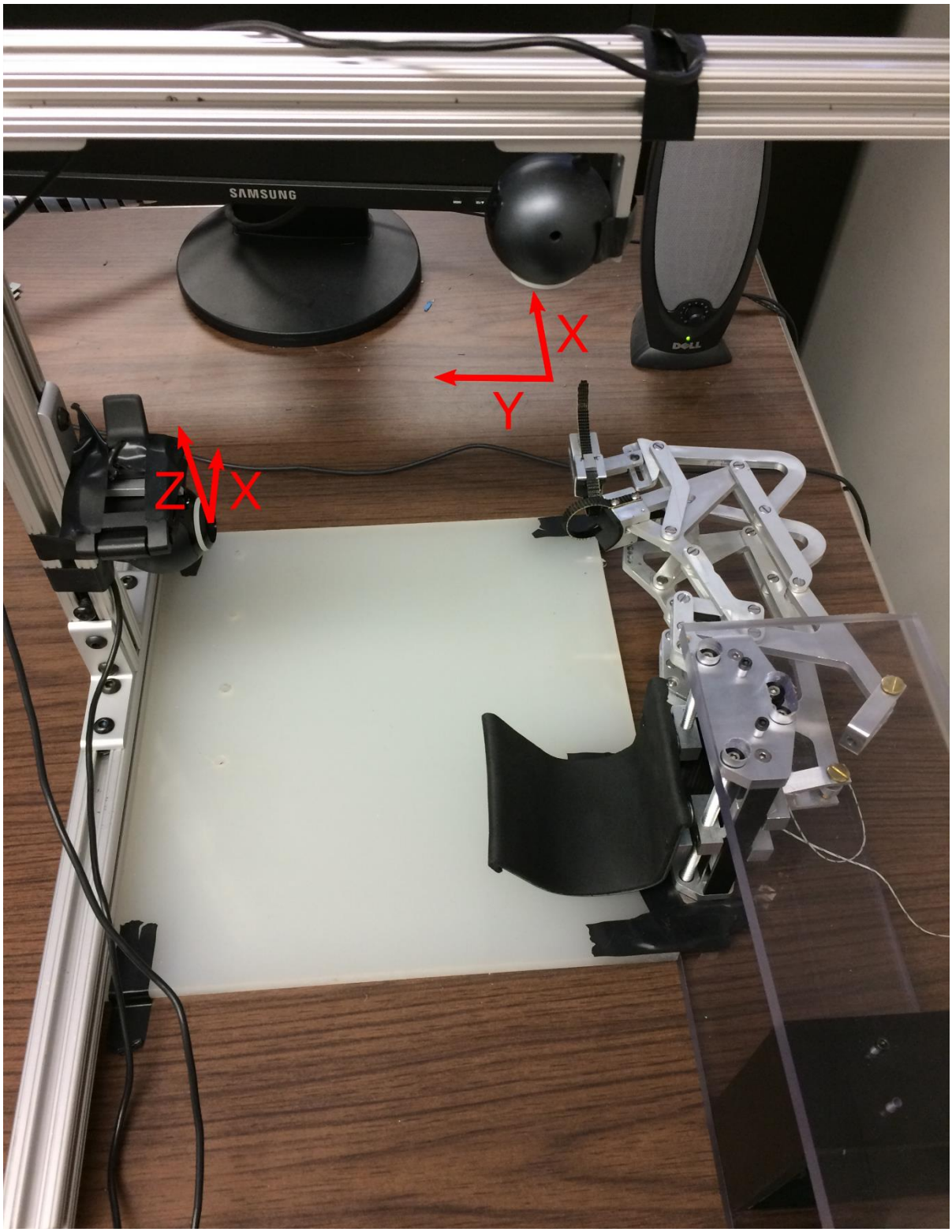


Figure 4. Motion tracking apparatus with two cameras on an aluminum frame and FINGER mock-up. Axes associated with local camera coordinate system shown in red on the figure.

The cameras were positioned orthogonally to each other with the upper camera obtaining a top view of the hand and thumb, while the lower camera obtained a side view. The top view was mirrored over the x-axis to orient the y-axis so it was consistent with a right-handed coordinate system. Examples of these views are shown in Figures 5 and 6.

For the three-dimensional reference frame, the green marker in Figures 5 and 6 was used as the origin. A right handed coordinate system was constructed in which x runs from the posterior to the anterior part of the arm and hand in both figures. The y-axis runs laterally from the dorsal to the ventral side of the hand in the top view in Figure 5. The z-axis runs vertically from the lateral side of the hand to the medial side in the side view in Figure 6.

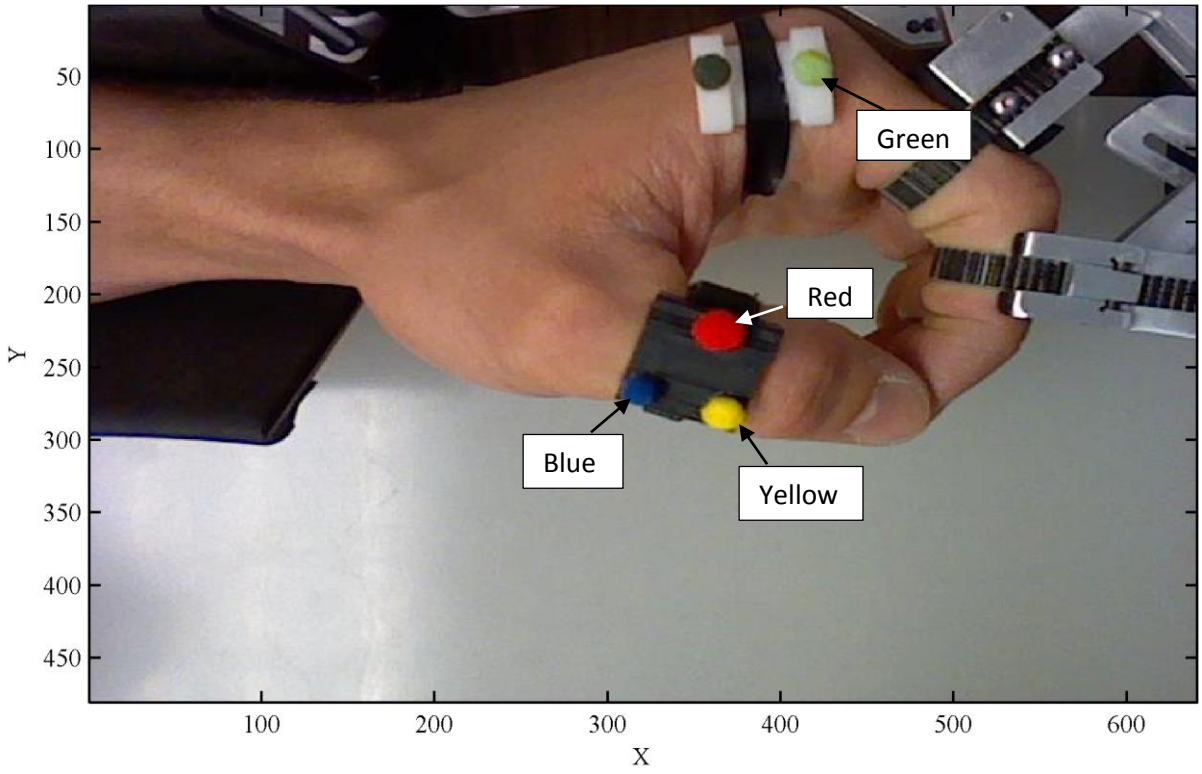


Figure 5. Top view of hand during motion tracking. This view shows displacement in the x-y plane. Units are in pixels.

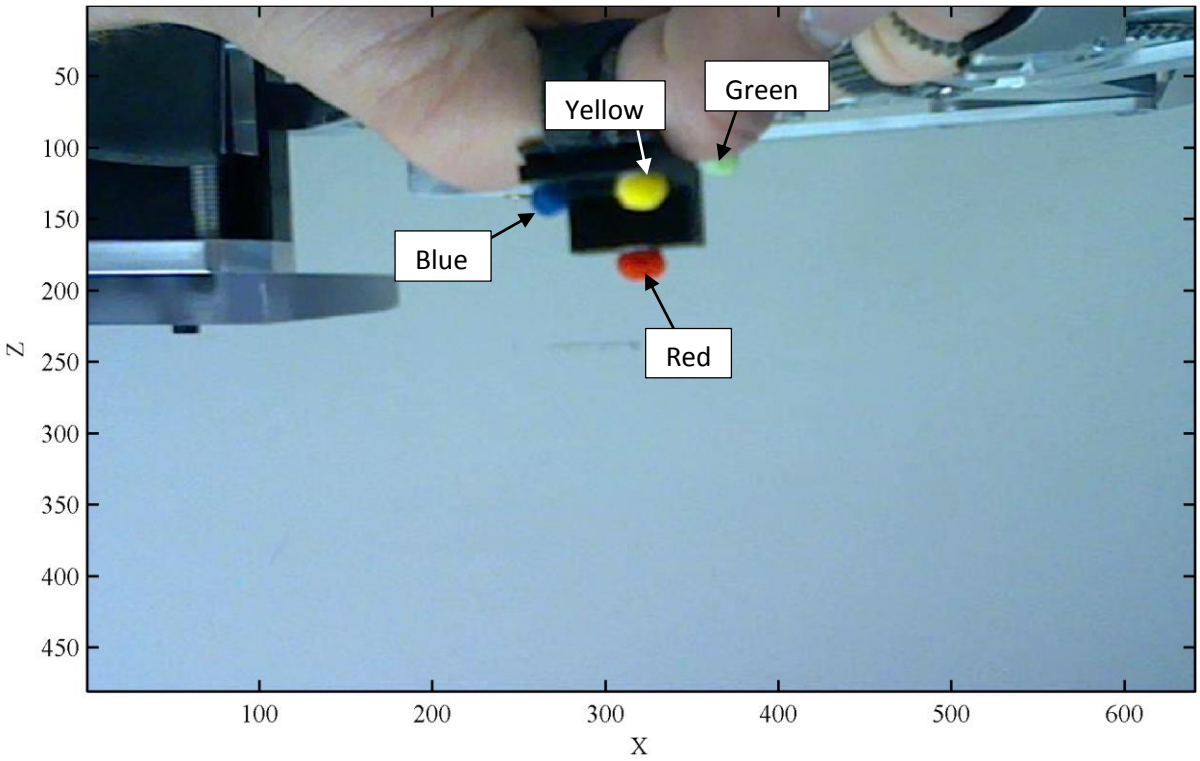


Figure 6. Side view of hand during motion tracking. This view shows displacement in the x-z plane. Units are in pixels.

## 2.3 Video Acquisition

The Matlab Image Acquisition Toolbox was used to obtain images from both cameras during motion tracking. During image acquisition, it is important that the area is well lit to provide necessary exposure for the cameras to achieve the desired frame rate. Before tracking, the subject donned the marker frame on the middle phalanx of the thumb and fixed the origin marker to the medial side of the metacarpophalangeal joint of the hand being tracked. (i.e., the right hand.) Then the wrist was placed in the wrist brace and the index finger was strapped into the exoskeleton of the FINGER mock-up. The position of the hand before tracking is shown in Figure 7.

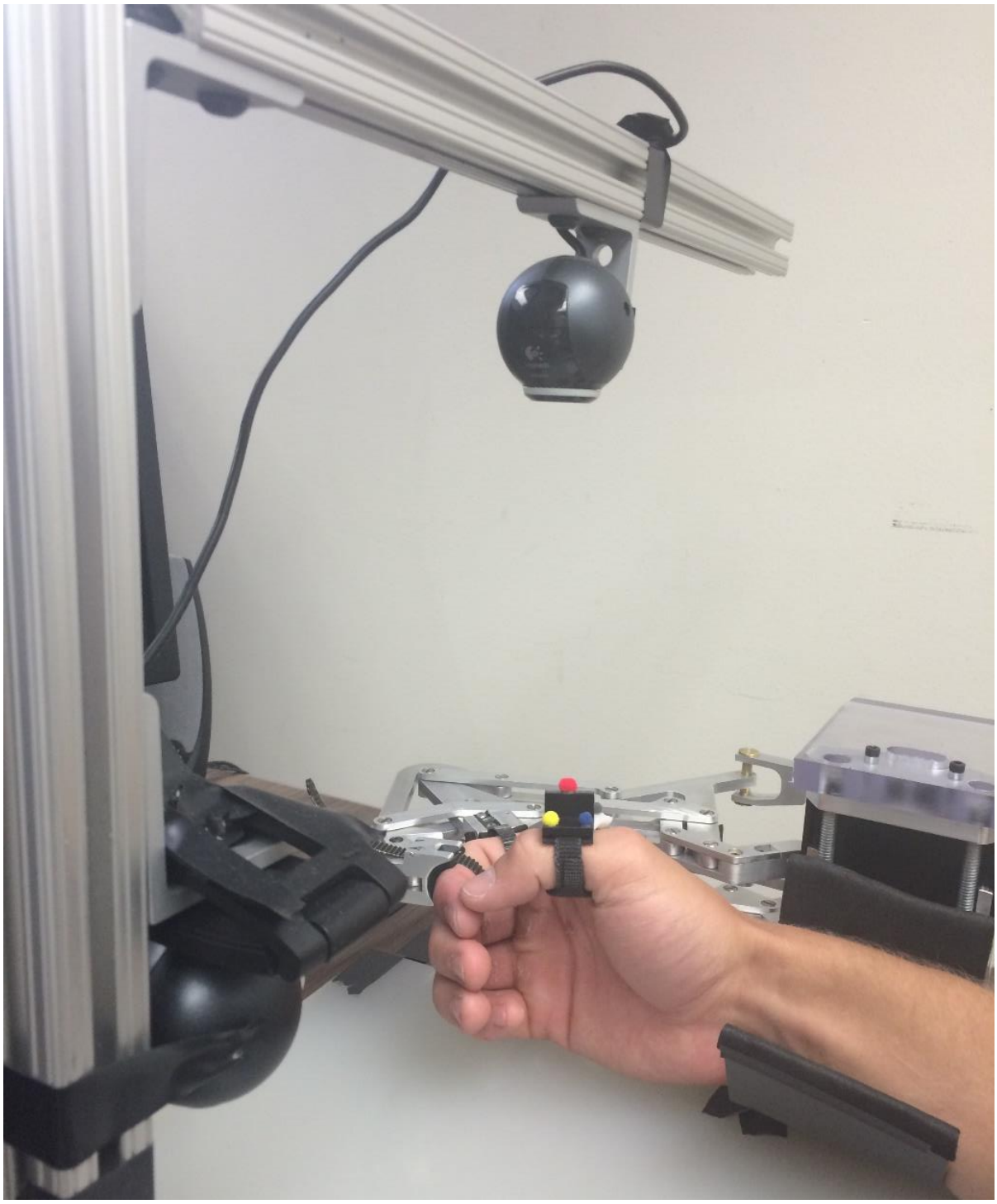

Figure 7. Setup showing hand with markers attached to FINGER and top and side cameras as well.

The subject waited for a visual cue in the Matlab command window indicating the cameras had started running, then began to flex and extend the thumb through the tip pinch grasp motion at a self-regulated pace. The thumb was tracked at 30 frames per second for 10 seconds after which the subject was instructed to stop.

## 2.4 Video Processing

The locations of each unique color were extracted from each frame using a Heaviside function. This function searched the frame for pixels with RGB values that matched the RGB values of the markers within a predefined range. The marker RGB values were calibrated for each video to account for changes in lighting. This procedure created two sets of images. One set was associated with the side camera, while the other set was associated with the upper camera.

## 2.5 Model of Thumb Motion

After the motion tracking data from the side and upper cameras were spliced together using the shared x-values, a curve was fit to each color. A slight shift existed between the x-values in the top and side views. This shift was removed by finding the average difference between the x-values in the two views. The x-values of the top view were shifted to be in the same range as those of the side view by adding the average difference to the original top view x-values.

The mean length between the blue and yellow markers in the motion capture was found to be 50.8 pixels. Due to errors in both the tracking and the modelling, the distance between the markers varied over the 11 sampled locations, so the standard deviation of the blue-yellow distance was 6.3 pixels. The same values for lengths between the yellow and red,

then, blue and red markers were 73.9 pixels and 8.0 pixels, and 78.4 pixels and 4.98 pixels respectively.

While the yellow-red and blue-red marker distances were found to both be approximately equal to 18.5 mm, the same distances had different average values when sampled from the motion tracking. It was assumed that the offset position of the red marker may have introduced distortion errors that caused this inconsistency, as the red marker had a significantly different relative distance to the cameras compared to the other markers. For this reason, the blue-yellow distance was used to find the conversion from pixels to millimeters. Dividing the distance between the blue and yellow markers, which was measured as 13.3 mm, by the mean distance between the same markers in pixels, which was 50.8 pixels, resulting in a conversion factor of 0.26 millimeters per pixel.

Polynomial regression was used to find the coefficients of a curve that modelled the trajectory of each color through flexion and extension. The fitted model used quadratic equations of the form:

$$[X][c] = [Y]$$
$$[1\ x\ y\ x^2\ y^2][c] = [z] \quad (1)$$
$$c = (X'X)^{-1}X'Y.$$

The equations for the z-value of each color are:

$$z_{blue} = -21.8 - 1.19x + 1.18y - 0.0119x^2 - 0.0193y^2$$
$$z_{red} = 8.97 - .972x + 0.389y - 0.0105x^2 - 0.009y^2 \quad (2)$$
$$z_{yellow} = -24.3 - 1.44x + 1.66y - 0.0161x^2 - 0.0239y^2.$$

The range of x and y values that cover the valid range of inputs for these equations are in Table I. The valid range was determined by maximum and minimum position for each color during tracking.

Table I. Bounding range of input values for equations that describe movement of markers. Values in millimeters.

| **Color** | $x_{min}$ | $x_{max}$ | $y_{min}$ | $y_{max}$ |
|---|---|---|---|---|
| Blue | -55.1 | -22.2 | 25.8 | 57.8 |
| Red | -46.9 | -10.5 | 6.21 | 49.4 |
| Yellow | -45.0 | -12.1 | 29.1 | 62.3 |

The regression with the quadratic equations produced a good fit for the trajectory of each color. The coefficient of determination (or $R^2$) for the blue track was 0.982. The $R^2$ value for the red and yellow tracks were 0.976 and 0.987 respectively.

The visual results of the regression against the raw data are shown in Figure 8. The small markers represent the raw data and the solid lines represent the curve fit to each set of color data. The green triangles symbolize the plane formed by the three markers on the motion tracking frame. Figure 8 also includes an image of the thumb being tracked by the side camera to provide a visual frame of reference. The image has been flipped to match the orientation of the thumb in the picture with the orientation of the characterized thumb path.

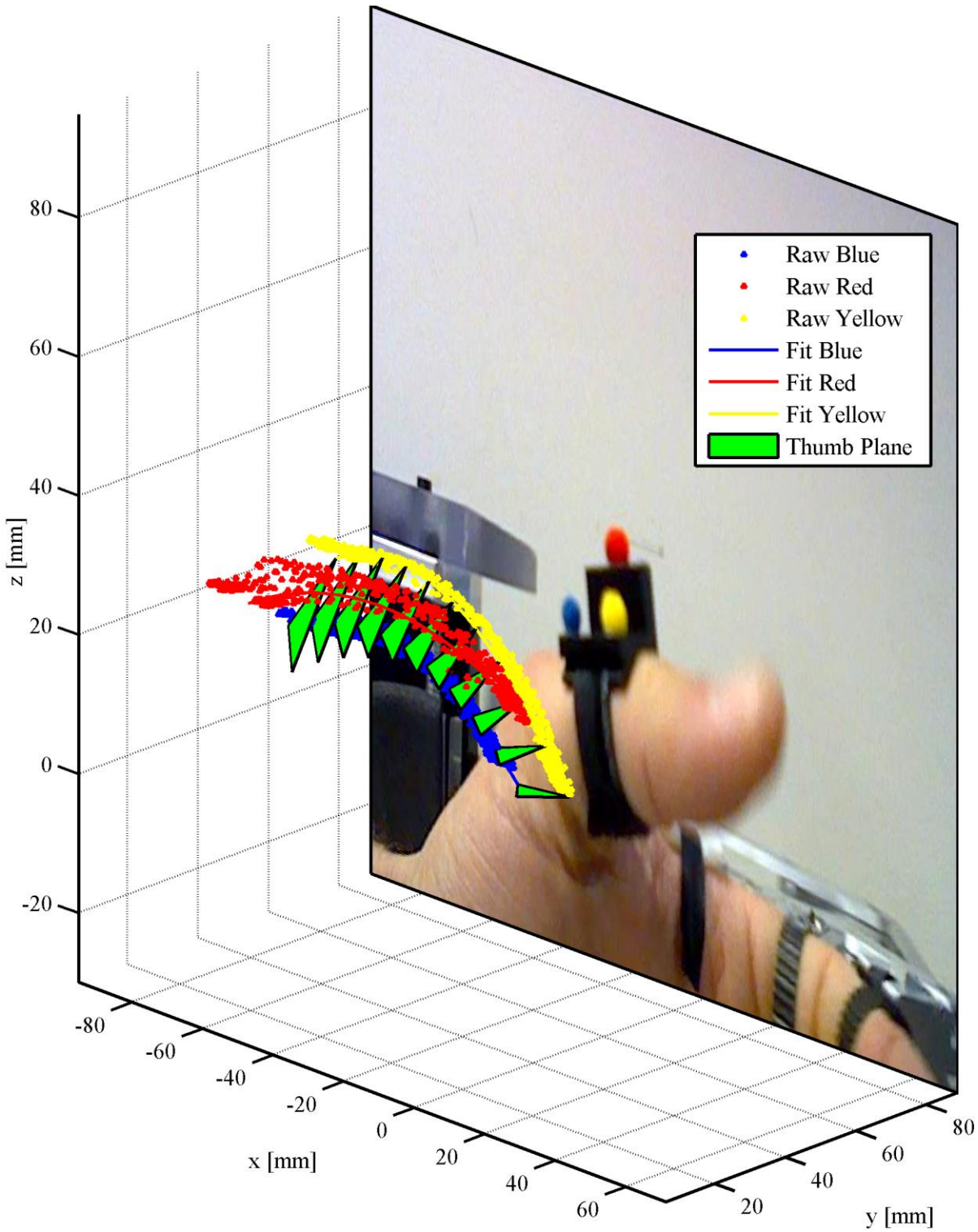


Figure 8. Raw tracked data as the small markers with a line representing the curve fit to each color. Figure also shows the plane of the marker frame with the green triangles (on which more information is given in Figure 9) and a mirrored side view from a camera. Units are in millimeters.

The point of the triangle associated with the red marker does not appear to follow the curve fit to the red marker in Figure 8 because that point has been transformed to remove the offset of the red marker relative to the blue and yellow markers. This transformation was the result of rotating the red marker about the axis running through the blue and yellow markers by the angle created by the horizontal and vertical offsets of the red marker from the blue and yellow markers on the frame as shown in Figure 3.

This oriented the marker plane parallel with the surface of the marker frame to which the blue and yellow markers were already fixed, as shown in Figure 9. Consequently, the plane represented by the green triangle in Figure 9 was parallel to the dorsal part of the thumb to provide information about the orientation of the thumb. The triangle extends beyond the marker frame as the geometry of the triangle was preserved during the rotation that placed it level with the surface on which the blue and yellow markers are fixed.

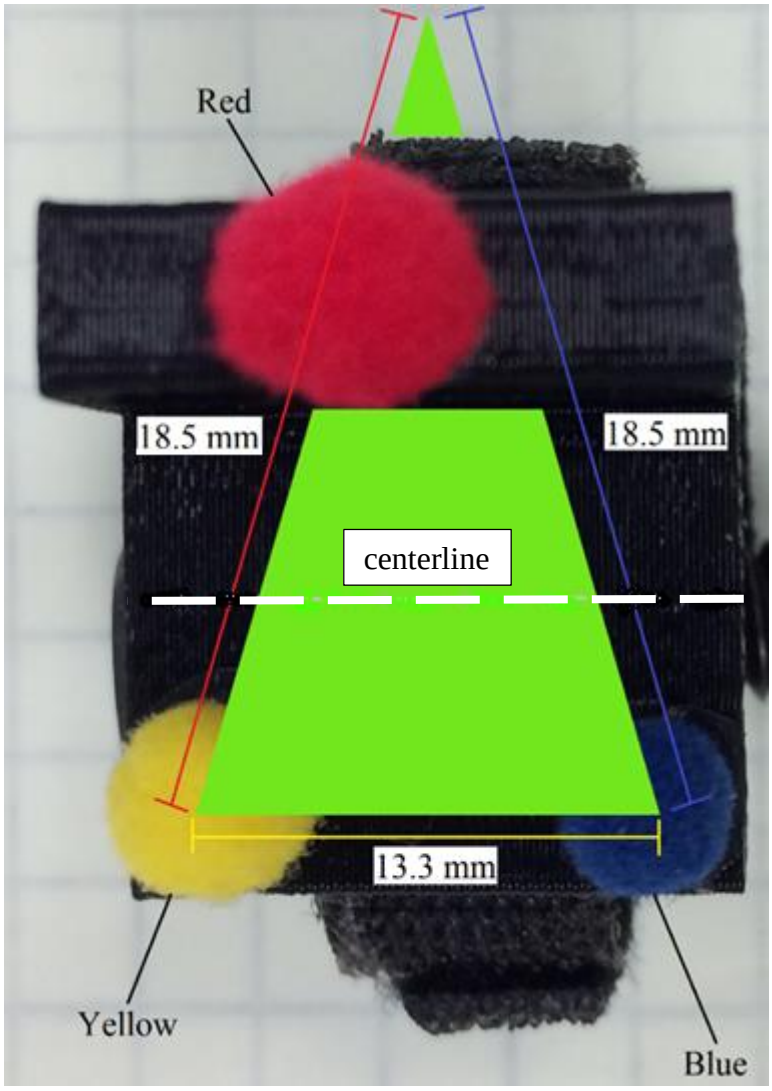


Figure 9. Top view of marker frame showing triangle representing the plane offset from the back of the thumb that is the result of rotating the red marker level with the surface on which the blue and yellow markers sit. The length of each side of the marker is also given in millimeters. A gray dashed line represents the centerline along the back of the thumb.

Having oriented the marker plane to match the orientation of the dorsal side of the thumb, a pair of points was translated in the marker plane from the blue and yellow markers respectively to the centerline of the thumb, which is denoted as a gray dashed line in Figure 9. Once translated, these points could be sampled for use as target points for mechanism synthesis. The two nodes on the end-effector are evaluated against these points during mechanism synthesis.

This pair of points was sampled 11 times at equal intervals along the trajectory of the thumb to create a set of target data points for mechanism synthesis. These target points are shown as red circles at all 11 locations in Figure 10. The points are also included in Appendix A.

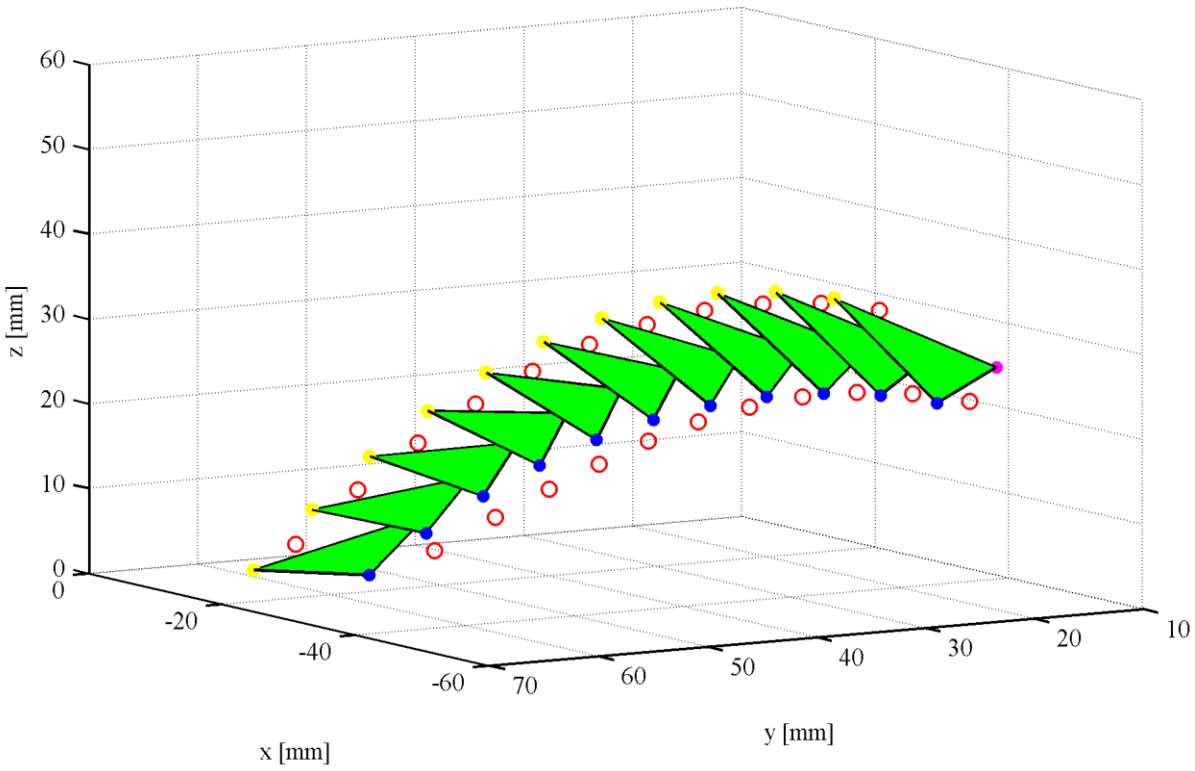


Figure 10. Target points represented by red circles and the plane in which the target points reside represented by green triangles through all 11 target configurations. Triangle vertices have blue, yellow, and magenta dots according to the color of the marker tracked by that vertex. (Note: the magenta dot is at the location of the red marker after the transformation from its tracked location.)

As variation existed between the 11 distances from the yellow to the blue markers, the distance between one set of target points was not necessarily the same as the distance between any other pair of points. Unmodified, this may have reduced the accuracy of the mechanism synthesis procedure since the end-effector would have likely fit pairs of points that had lengths closer to the mean value better than those pairs that were further from the mean length. This could have introduced undesirable behavior in the mechanism, such as over-emphasizing target pairs closer to the mean length, as it fit a fixed-length end-effector to

target points with variable distances rather than simply fitting the end-effector position to the path of the thumb. This situation was fixed by adding or subtracting lengths to and from the markers along the vector running through the markers. This set all of the distances between each marker pair equal to 13.3 mm, which was the distance between the blue and yellow markers.

This simplified the search space for the optimization of the mechanism by providing a fixed distance between the markers for the end-effector nodes to match. Finally, the positions of all the target points were adjusted with respect to the origin determined by the location of the green marker, shown in Figures 5 and 6, in the first frame during the motion tracking. Since the distance from the closest corner of the FINGER mock-up to the location of the marker in the first frame was known, the path of the thumb could be reckoned with respect to the housing for FINGER to assist in the design of the mechanism by using this origin as a reference.

# Chapter 3. Mechanism Synthesis

## 3.1 Introduction

This chapter covers the procedure of mechanism synthesis used to find a solution for a mechanism that would follow the trajectory of the thumb. Mechanism synthesis is the process of determining the mechanism parameters for a mechanism that follows a set path. In this case, the 11 pairs of points sampled from the thumb path data formed the desired target path.

Several methods of mechanism synthesis exist for linkages including graphical and closed-form methods. With modern computational power it is now possible to synthesize mechanisms with optimization techniques such as function minimization. This project used function minimization to find a set of mechanism parameters so that the end-effector of the linkage would follow the desired target path. This set of parameters forms a kinematic solution that can then be used as the basis for the design of an exoskeleton for rehabilitation of the thumb after stroke.

The thumb mechanism exoskeleton described herein is designed to control the position and angle of the middle phalanx of the thumb during a naturalistic grasping motion. It is designed as a planar mechanism with a single-degree-of-freedom. The form of the mechanism is a Watt Type I. This six-bar type is similar in form to the eight-bar type used in FINGER.

The distal phalanx is left free, as in the case of FINGER, to allow for tactile feedback during therapy. The mechanism is further designed to remain behind the thumb and above the wrist throughout the full range of motion. This simplifies donning the device. More

importantly, it makes the device safe to use since the exoskeleton is mechanically constrained to stay out of the space occupied by the thumb and arm.

## 3.2 Mechanism Parameters

The variables optimized during mechanism synthesis can be divided into two categories. The first category includes the variables for the planar mechanism kinematics. The second category includes variables for the mechanism plane. The planar mechanism variables include the lengths of the mechanism links, $d_{1\text{-}9}$, the three-dimensional Cartesian location of the ground nodes, G and $G_1$, and the structural angles of the mechanism, $\alpha$, $\beta$, $\gamma_1$, and $\gamma_2$. An input angle $\theta_1$, located at node G and measured from the line $\overline{GG_1}$, was also found for each of the 11 configurations. These variables are shown in Figure 12.

The variables for the mechanism plane described the location of the origin of the plane and the orientation of the plane. The plane was oriented using the ZXZ Euler angles, $\alpha$, $\beta$, and $\gamma$. These variables formed the rotation matrix:

$$R = \begin{bmatrix} c\gamma c\alpha - s\gamma c\beta s\alpha & -s\gamma c\alpha - c\gamma c\beta s\alpha & s\beta s\alpha \\ c\gamma s\alpha + s\gamma c\beta c\alpha & -s\gamma s\alpha - c\gamma c\beta c\alpha & -s\beta c\alpha \\ s\gamma s\beta & c\gamma s\beta & c\beta \end{bmatrix}. \quad (3)$$

The three-dimensional Cartesian location of the origin of the plane was defined by $p_x$, $p_y$, and $p_z$. Figure 11 shows the mechanism plane transformed by the translation and rotation variables.

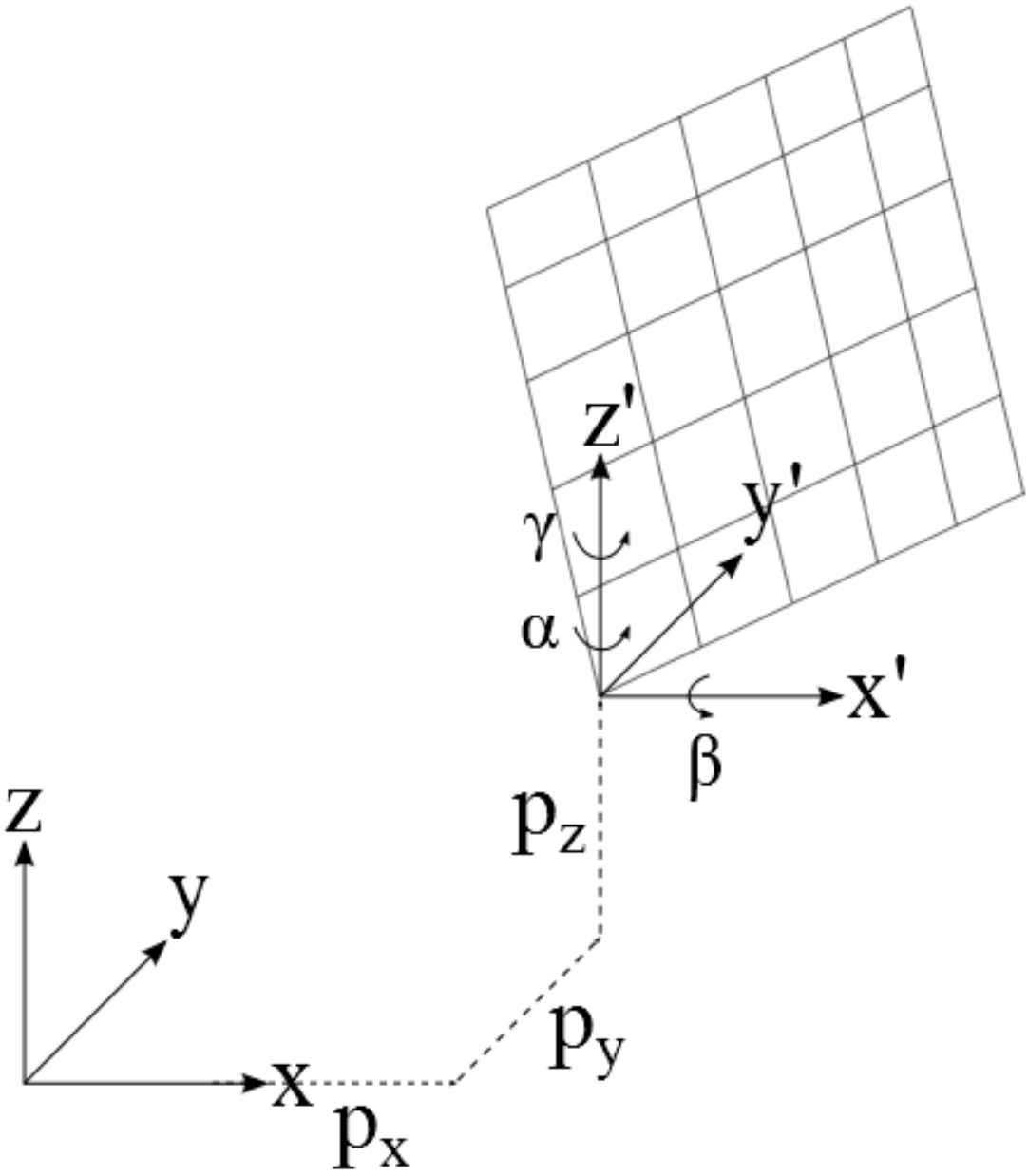


Figure 11. Mechanism plane shown with respect to origin x, y, z along with translating parameters px, py, and pz and Euler angles α, β, and γ for rotation about local frame x', y', z'.

The motion of the mechanism was solved using forward kinematics in a similar manner to the procedure used in [39]. This allowed the location of each node in the mechanism to be found given a set of structural parameters and a single driving input angle. The complete kinematic equations that solve for the locations of the upper ($M_2$) and lower

(M) nodes on the end-effector can be found in Appendix B. However, the equations that describe the kinematics of the base four-bar mechanism are:

$$\begin{aligned}
\angle GG_1 &= atan2(G_{1y} - G_y\,, G_{1x} - G_x) \\
\boldsymbol{A} &= \boldsymbol{G} + d_1 \begin{pmatrix} sin \\ cos \end{pmatrix} (\angle GG_1 + \theta_1) \\
\angle AG_1 &= atan2(G_{1y} - A_y\,, G_{1x} - A_x) \\
\overline{AG_1} &= \sqrt{\overline{(A_y - G_{1y})^2 + (A_x - G_{1x})^2}} \\
\angle G_1AB &= \text{acos}\left((\overline{AG_1}^2 + d_2^2 - d_3^2)/2\overline{AG_1}d_2\right) \\
\boldsymbol{B} &= \boldsymbol{A} + d_2 \begin{pmatrix} sin \\ cos \end{pmatrix} (\angle G_1AB - \angle AG_1)
\end{aligned} \tag{4}$$

The variables used in Equation (4) and used to solve the kinematics for the remainder of the six-bar mechanism are shown on the mechanism in Figure 12. These variables include the structural lengths, $d_{1\text{-}9}$, and angles, $\alpha$, $\beta$, $\gamma_1$, and $\gamma_2$, the base node locations G and $G_1$ and the input angle $\theta_1$, which along with angle $\angle GG_1$, defines the configuration of the mechanism.

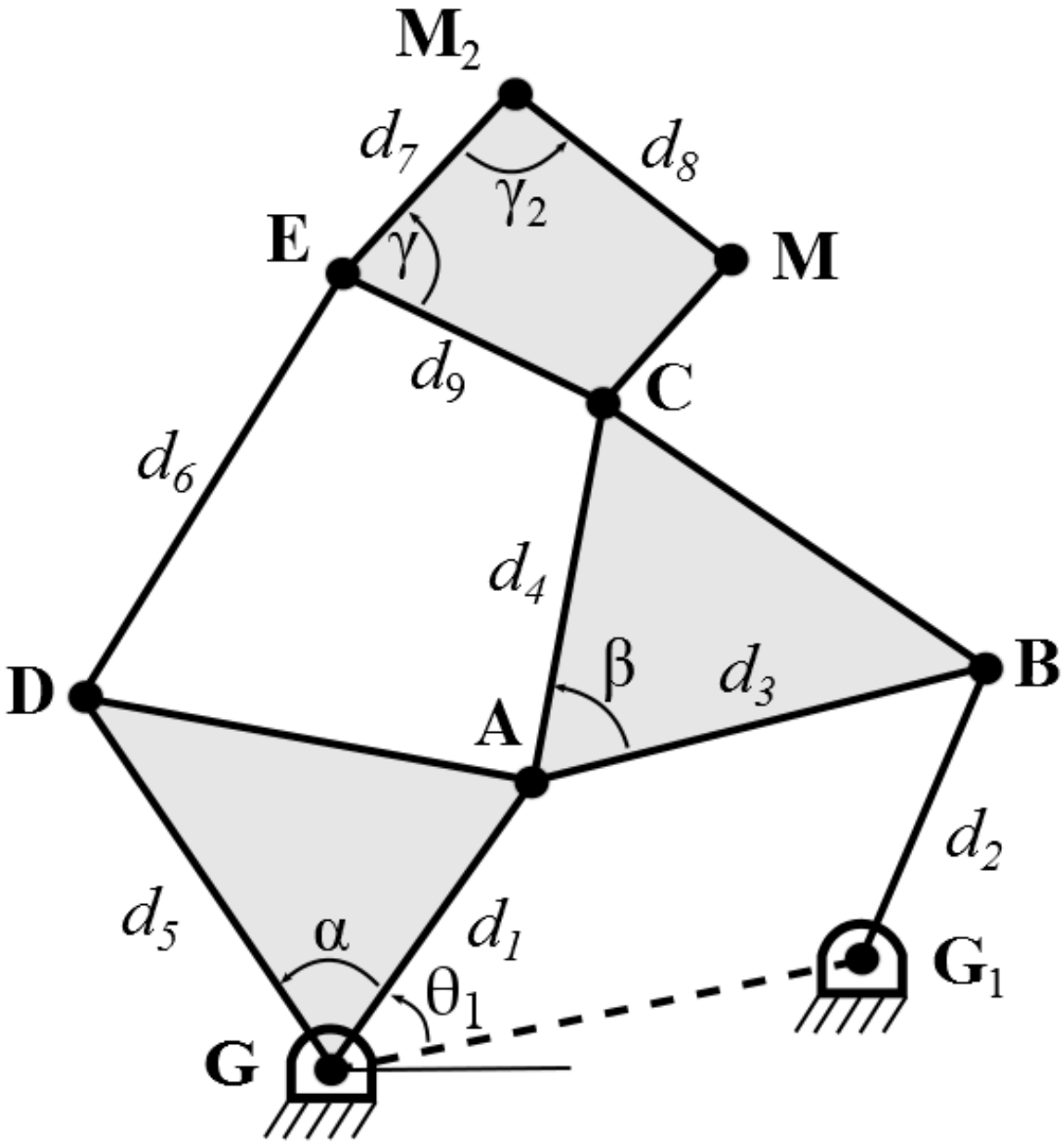


Figure 12. Mechanism with structural parameters and input angle $\theta_1$.

## 3.3 Objective Function Minimization

The optimization procedure uses a constrained nonlinear multivariable function minimizer (Matlab's 'fmincon') for mechanism synthesis. An objective function was constructed for the optimization that quantified the error in the mechanism and the effect of various penalty constraints. The full form of the objective function is:

$$J = J_M + J_{M_2} + J_f + J_{jo} + J_{ti} + J_h \tag{5}$$

where $J_M$ and $J_{M2}$ are error terms and $J_f$, $J_{jo}$, $J_{ti}$, and $J_h$ are penalty terms.

The primary terms in the objective function are the sum of the squared error between the mechanism end points M and $M_2$ and the goal thumb points T and $T_2$ which are the desired target points along the thumb trajectory path. The error was summed over the range of the 11 pairs of target points representing the trajectory of the thumb. The equations for the error between the mechanism end nodes (M and $M_2$) and the target points (T and $T_2$) are:

$$\begin{aligned} J_M &= \sum_{n=1}^{11} |\boldsymbol{T} - \boldsymbol{M}|_n \\ J_{M_2} &= \sum_{n=1}^{11} |\boldsymbol{T_2} - \boldsymbol{M_2}|_n \end{aligned} \tag{6}$$

The objective function also included four penalty constraints. These constraints avoided infeasible mechanisms, joint overlap, and unsafe interference with the patient. Infeasible mechanisms occur when the links are not sized correctly in relation to each other to create a complete loop. When this happens the angle $\angle G_1AB$ or $\angle CDE$ across the quadrilateral formed by the links of one of the four bars that make up the six bar in Figure 12 is a complex number. Any solution with complex angles in any configuration during its motion along the path was given a large penalty to its fitness so it was very unlikely to be considered a good solution. The equation for the constraint is:

$$J_f = K_f \sum_{n=1}^{11} (top + bottom), \tag{7}$$

where $K_f$ is the feasibility coefficient, upper refers to the four bar consisting of nodes DACE in Figure 12, and lower refers to the four bar $GABG_1$ in the same figure. If an angle related to either the upper or lower four bars is complex the respective variable is given a value of one, otherwise both variables equal zero and no penalty is added for that configuration.

The penalty for joint overlap keeps all the joints at least 10 mm apart. Since the bearings in the mechanism will have a 6.35 mm outer diameter a minimum of about a 3.65 mm of material will separate the bearings. These dimensions follow the practice used in designing FINGER [40].

The joint overlap was calculated using the Euclidean norm between each unique joint at each step of the mechanism during rotation. At each step, any distance greater than 10 mm was ignored. If distances less than 10 mm were found, the difference between 10 mm and the smallest value was returned to be used in the penalty. In this manner, joint differences less than 10 mm increased the value of the objective function. So the total joint overlap penalty is defined as:

$$J_{jo} = K_{jo} \sum_{n=1}^{11} \max[\sum_{i=1}^{8} \max(0, offset - |\boldsymbol{P_{n,i}} - \boldsymbol{P_{n,i+1}}|)], \quad (8)$$

where $K_{jo}$ is the penalty coefficient, offset is the threshold joint difference, and the location of each joint is P. The thumb interference penalty kept all the mechanism joints, with the exception the nodes M and $M_2$ on the end effector, above the thumb by at least 10 mm. This penalty prevented any part of the mechanism from intersecting the thumb during motion. This keeps use of the robot comfortable and safe for the patient.

Since the markers were already about 5 mm off the back of the thumb, the 10 mm total offset from the back of the thumb was achieved by adding a 5 mm offset to the original position of the markers. After the mechanism synthesis the end nodes on the end effector, M

and $M_2$, are approximately positioned 5 mm off the back of the thumb since those nodes tracked the markers which were displaced 5 mm from the back of the thumb. This provided space to construct the thumb interface during the mechanical design of the exoskeleton.

The distance between the other nodes and the plane of the markers was calculated in each configuration using the three dimensional Euclidean distance. If any of those distances were less than 5 mm, the difference between 5 and that distance value was summed to be multiplied by the penalty factor. So the total penalty for thumb interference is the sum of the product of the summed distances and the penalty coefficient through all eleven configurations is defined as:

$$J_{ti} = K_{ti} \sum_{n=1}^{11} \sum_{i=1}^{7} \max(0, offset - |\boldsymbol{T_{n,i}} \cdot \boldsymbol{P_{n,i}}|/|\boldsymbol{T_{n,i}}|), \quad (9)$$

where $K_{ti}$ is the thumb interference penalty, offset is the threshold displacement, T is the location of a point on the thumb plane, and P is the location of a joint. The mechanism was kept off the back of the wrist or arm in a similar manner. Specifically, the distance between the height (in the z-direction) of the bottom marker, T, in full flexion (the lowest position of the thumb) and every joint in the mechanism in each configuration was calculated. Any negative distances were summed and added to the penalty equation for each configuration. So the total penalty to keep the mechanism above the hand is the sum of the sum of all the distances between the marker and each joint when the vertical joint position is less than that of the marker in all eleven configurations as defined by:

$$J_h = \sum_{n=1}^{11} \sum_{i=1}^{9} \max(0, \min(z_{thumb_1}) - z_{joint_{n,i}}), \quad (10)$$

where $z_{thumb}$ is the vertical position of the thumb and $z_{joint}$ is the vertical position of the joint

In addition to the penalties used to control mechanism behavior, bounds were placed on the mechanism parameters. These bounds ranged from -120 to 150 for all variables. The

units are millimeters for the structural variables and radians for the angles. This range gave freedom to the angle variables to go around the unit circle as necessary, while placing hard stops on the lengths of the mechanism parameters keeping the mechanism size and position in the mechanism plane reasonable.

A pure random search method was used to examine as many potential solutions as possible. In order to avoid wasting computational time attempting to synthesize significantly infeasible mechanisms the initial conditions for the solutions were generated between set bounds. These bounds were specific to the type of parameter and are shown in Table II.

Table II. Parameter bounds for initial conditions.

| **Bounded Initial Conditions** | | |
|---|---|---|
| Parameter | Min | Max |
| $G_x$ and $G_{1x}$ | 0 mm | 80 mm |
| $G_y$ and $G_{1y}$ | 0 mm | 50 mm |
| Length ($d_{1\text{-}7}$) | 30 mm | 80 mm |
| $P_x$ | 0 mm | 20 mm |
| $P_y$ | 40 mm | 50 mm |
| $P_z$ | 30 mm | 40 mm |
| Structural angles ($\alpha$, $\beta$, $\gamma$, $\gamma_2$) | 0 | $\pi/3$ |

A few parameters had values that were known to be close to a specific value. Consequently, these parameters were not randomly generated. Instead they were fixed at the values shown in Table III.

Table III. Parameters for fixed initial conditions.

| **Fixed Initial Conditions** | |
|---|---|
| Parameter | Value |
| Input angles ($\theta_1$) | 0 |
| Euler angles ($\alpha$, $\beta$, $\gamma$) | 0.014, 0.13, 0.146 |

# Chapter 4. Mechanism Selection

## 4.1 Introduction and Criteria

The procedure of mechanism synthesis found many unique local minima producing a large number of distinct solutions with a total error between 17 and 18 mm. For all these potential solutions, the error was mostly the result of out of plane error. However, selecting a final solution for the exoskeleton mechanism from the potential solutions required considering various design criteria. The process of selection was iterative as the solution selected from the first mechanism synthesis process was used as a foundational seed for a second round of focused mechanism synthesis to find the solution selected for the initial prototype.

The selection of a mechanism solution is driven by both kinematic and mechanical design requirements. Kinematic requirements include continuous movement and that solutions exist outside the space occupied by the housing for FINGER. Mechanical design requirements are largely regulated by routing the mechanism links so that they clear each other during the entire mechanism motion.

Designing the links so that they clear each other can create complex link geometry. This geometry can make potential solutions unsuitable for design. Some solutions have links that are so compact that no space exists to easily rout the links around each other. Other solutions have joints that transect links too significantly in certain mechanism configurations to be reasonably accommodated. Another non-viable link geometry requires links to be routed through the patient or the housing for FINGER to clear other links.

Mechanical design issues unrelated to link clearance include solutions that place the exoskeleton between the base joints G and $G_1$ and the thumb. This arrangement requires a

large addition to the driving link to provide an attachment point for the actuator to maintain the predicted mechanical advantage for the mechanism. Another problem is the drive link being located in a manner that would require the actuator to intersect the housing for FINGER or if the drive link is surrounded by other links in a way that made attaching an actuator difficult.

## 4.2 Mechanical Advantage

An important criterion for the exoskeleton is its mechanical advantage. Since the linear actuators used on FINGER and planned for use with this exoskeleton are not geared, the mechanical advantage of the mechanism is the only avenue for force amplification. Therefore, it is important to find the mechanism with geometry that provides a relatively high mechanical advantage compared with the other potential solutions in the necessary mechanism positions. In this case the mechanism needs higher mechanical advantage in extension to counteract the tone frequently present in the hand of a patient.

The mechanical advantage over the range of the motion of the mechanism was evaluated by velocity analysis. Two unique curves were found by comparing the velocity of the top node of the input link with the output velocity of the end-effector nodes M and $M_2$. The velocity of the nodes was approximated by discretizing the movement of the mechanism and evaluating the change in distance of the nodes over incremental steps. Figure 13 shows the variables associated with calculation of the velocity of the nodes, and thus the mechanical advantage profile.

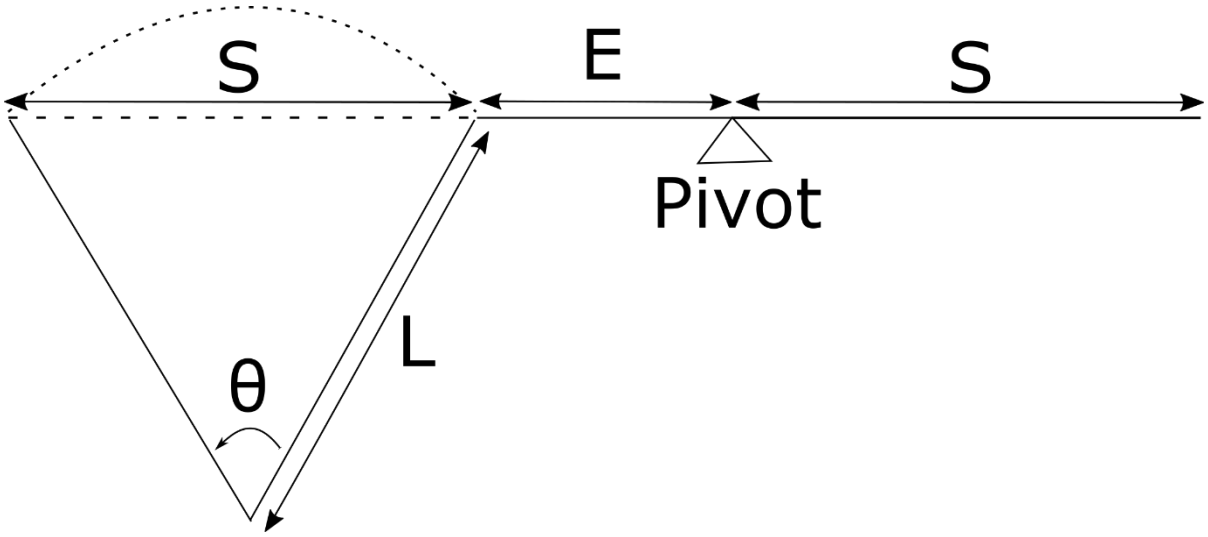


Figure 13. Figure describing calculation of mechanical advantage. S is the stroke length. E is the distance from the actuator pivot to the attachment of the actuator to the exoskeleton. L is the lever arm length. The total transmission angle is θ.

All the potential solutions were evaluated using dimensions from the linear actuator that will be used once the final mechanism is manufactured. These dimensions include a stroke length (S in Figure 13) of 142 mm. The distance from the actuator pivot point to the attachment of the actuator to the exoskeleton mechanism (E in Figure 13) is 110.9 mm. The stroke length was used along with the travel angle of the solution (θ in Figure 13) to find the distance from the base node G to the attachment of the actuator to the mechanism using the law of cosines. After this, the angle θ was discretized into 1000 angles that were input into the mechanism kinematic equations to find the linear displacements of the input and output nodes. Then these displacements could be used to determine the mechanical advantage curves by dividing the input node's displacement uniquely by each of the output nodes' displacements.

## 4.3 Results

Very few of the solutions initially found during the mechanism synthesis process were viable. Many mechanisms had low mechanical advantage in extension or alternatively had a mechanical disadvantage in flexion. A few solutions had very discontinuous motion,

while others had the driving link surrounded by other links in a manner that would make it impossible to attach an actuator. Problems associated with routing the links so that they cleared each other disqualified several other mechanisms. Still other solutions placed the exoskeleton between the base nodes and the thumb. Also, several solutions would have intersected the housing for FINGER.

Three solutions with good mechanical advantage appeared to meet the criteria discussed above. Those solutions are shown in extension below in Figures 14, 15, and 16 along with their end-effector trajectories overlaid onto the thumb trajectory. Both a front and a side view are shown for each mechanism. For future reference, the solution in Figure 14 will be referred to as Solution A, while the solutions in Figures 15 and 16 will be referred to as Solutions B and C, respectively.

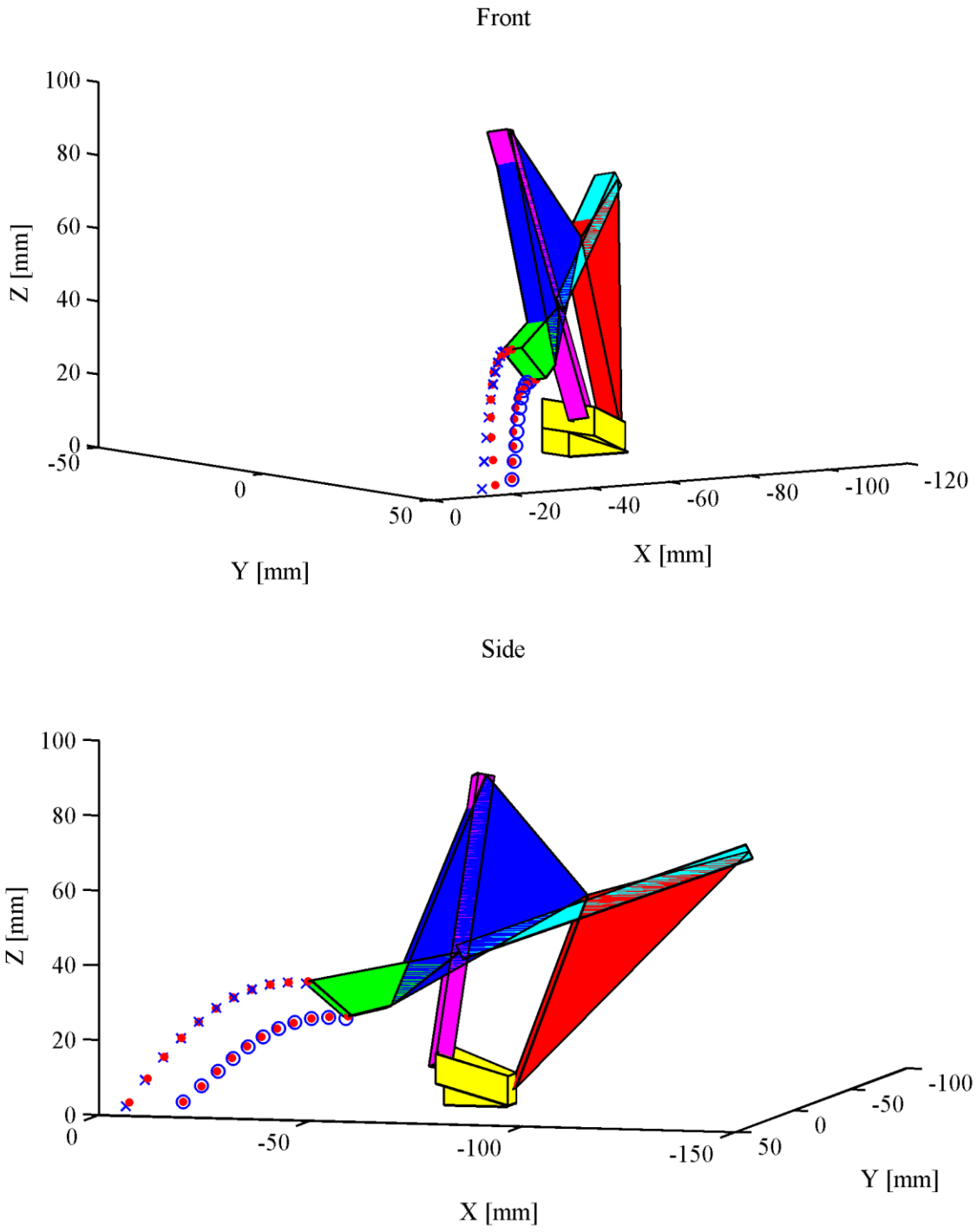


Figure 14. Front and side views of Solution A in full extension. The red dots trace the end effector path for all 11 configurations while the blue x's and o's trace the target path. All units are in millimeters.

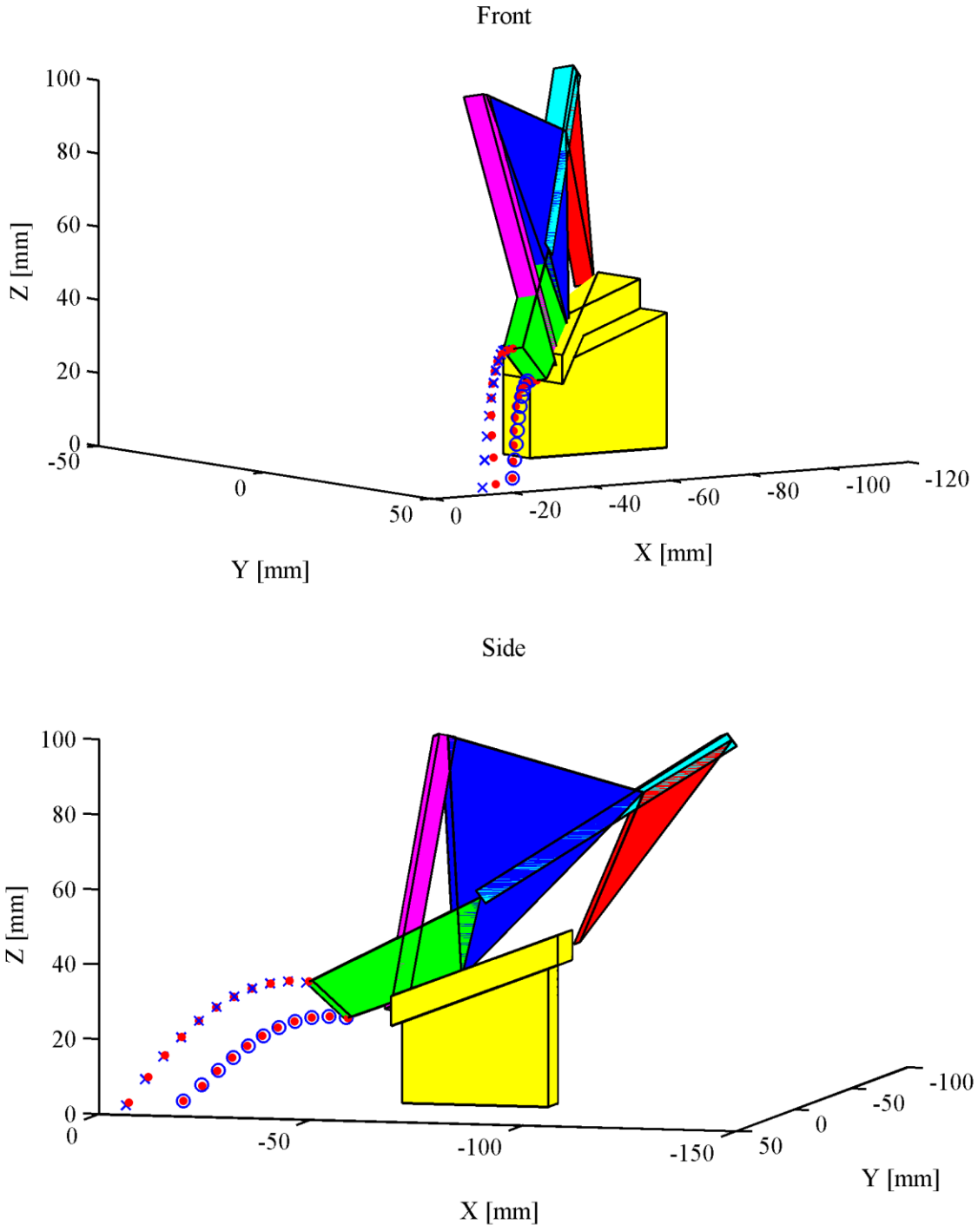


Figure 15. Front and side views of Solution B in full extension. The red dots trace the end effector path for all 11 configurations while the blue x's and o's trace the target path. All units are in millimeters.

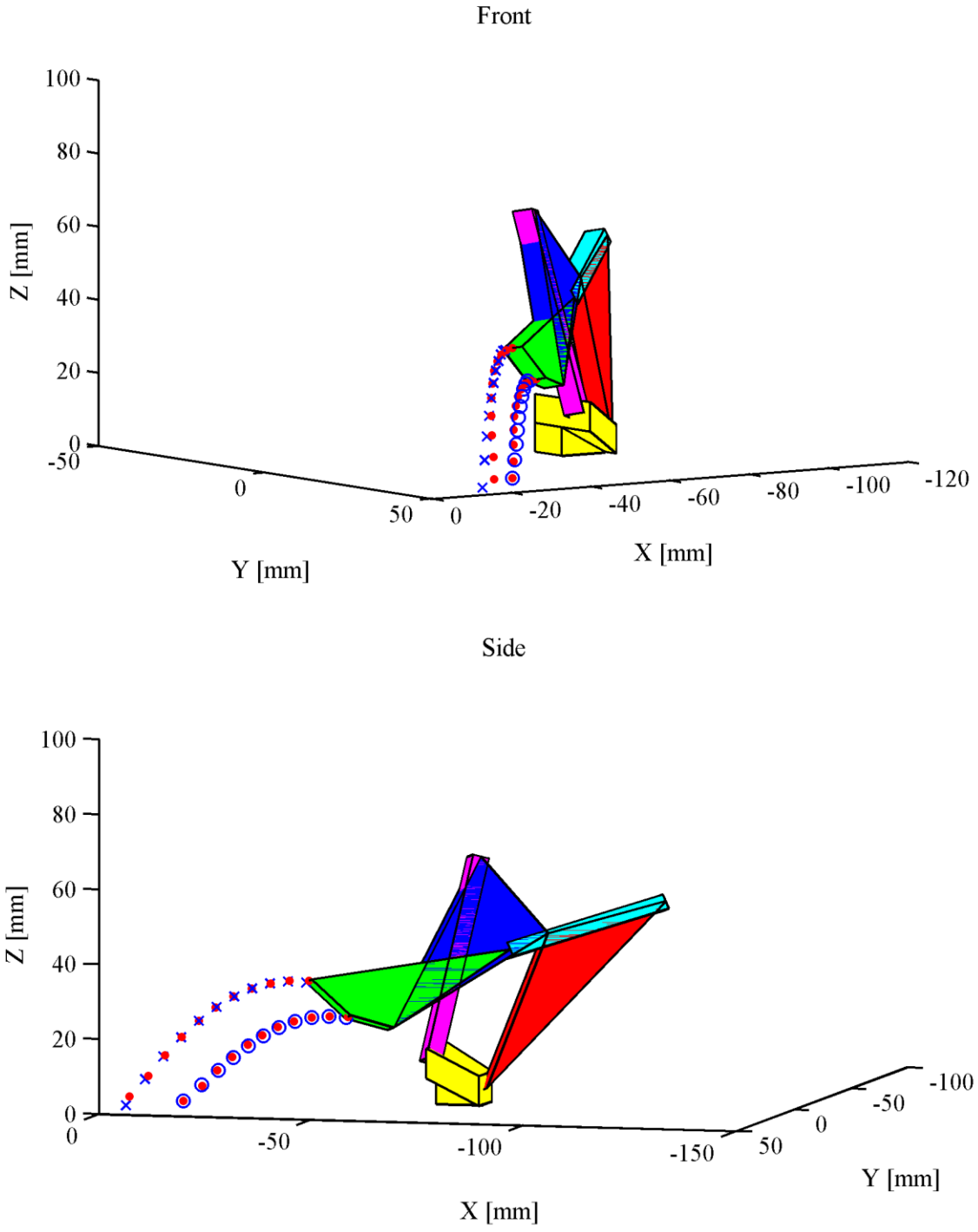


Figure 16. Front and side views of Solution C in full extension. The red dots trace the end effector path for all 11 configurations while the blue x's and o's trace the target path. All units are in millimeters.

The mechanical advantages for all three solutions are overlaid on Figure 17 below. The blue and green lines represent the mechanical advantage for nodes M and $M_2$ on the end-effector respectively. Solution A is represented by the solid line, while Solutions B and C are represented by the dashed and dotted lines respectively.

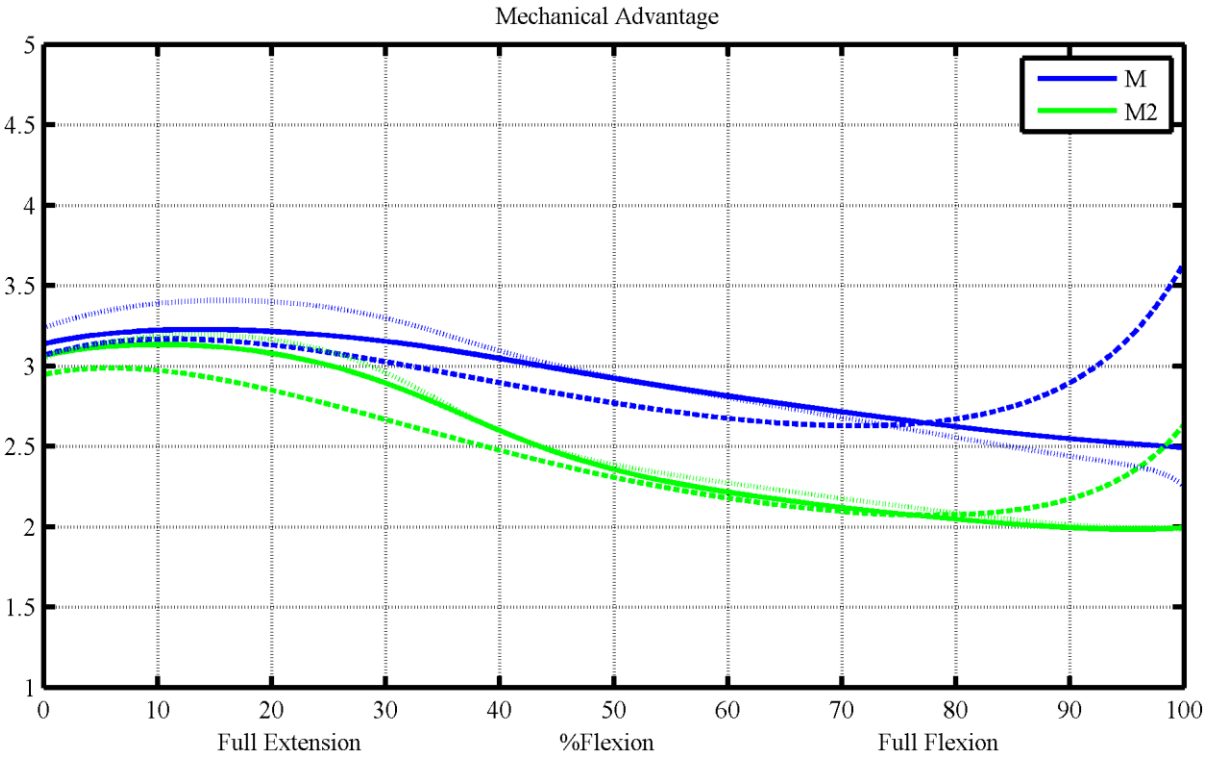


Figure 17. Mechanical advantage plot for three best mechanism solutions. The selected solution (A) is the solid line, while B is the dashed line and C is the dotted line. The blue lines represent the mechanical advantage evaluated at node M on the end-effector. The green lines represent the mechanical advantage evaluated at node $M_2$ on the end-effector.

Solution C has a slightly higher mechanical advantage in extension. Still, in full flexion its mechanical advantage begins to fall off more steeply than the other two solutions. Solution A has a somewhat linear slope over the majority of its range. Solution B has a large increase in mechanical advantage in flexion. Overall, though, the mechanical advantage profile for all three solutions was relatively similar.

Unfortunately, a closer inspection of all three solutions revealed that certain configurations placed some joints in troublesome locations. These locations would require thin links to avoid link intersection that would make the mechanism fragile. Since these

solutions were the best results from the mechanism synthesis, the next step was to select one and probe the search landscape around that solution for a more favorable result. Solution A was selected for the re-optimization since it had only one link that was significantly affected, while the other solutions had multiple links affected.

The values for this solution that were used as seeds in the refined optimization are in the tables below. The first column contains the lengths of each link in the structure. The second column contains the four structural angles. The third column shows the planar Cartesian coordinates of the location of the base nodes. The last column has the input angles for each configuration of the mechanism in order.

Table IV. Mechanism parameters and input angles for initial solution.

| Structural Lengths (mm) | | | Structural Angles (radians) | | | Base Locations (mm) | | | Input Angles (radians) | | |
|---|---|---|---|---|---|---|---|---|---|---|---|
| $d_1$ | = | 55.8578 | $\alpha$ | = | 0.3823 | $G_x$ | = | 0.8683 | $\theta_{1,1}$ | = | 1.6124 |
| $d_2$ | = | 39.6236 | $\beta$ | = | 4.7854 | $G_y$ | = | 17.1366 | $\theta_{1,2}$ | = | 1.5027 |
| $d_3$ | = | 79.7031 | $\gamma_1$ | = | 0.4849 | $G_{1x}$ | = | 17.5382 | $\theta_{1,3}$ | = | 1.4002 |
| $d_4$ | = | 57.8664 | $\gamma_2$ | = | 1.0044 | $G_{1y}$ | = | 24.6847 | $\theta_{1,4}$ | = | 1.3010 |
| $d_5$ | = | 87.9099 | | | | | | | $\theta_{1,5}$ | = | 1.2065 |
| $d_6$ | = | 77.0666 | | | | | | | $\theta_{1,6}$ | = | 1.1156 |
| $d_7$ | = | 37.2628 | | | | | | | $\theta_{1,7}$ | = | 1.0257 |
| $d_8$ | = | 13.1520 | | | | | | | $\theta_{1,8}$ | = | 0.9302 |
| $d_9$ | = | 22.6555 | | | | | | | $\theta_{1,9}$ | = | 0.8294 |
| | | | | | | | | | $\theta_{1,10}$ | = | 0.7210 |
| | | | | | | | | | $\theta_{1,11}$ | = | 0.5980 |

The next table contains the three-dimensional location of the mechanism plane in the first column along with the Euler angles that defined the orientation of the plane in the second column.

Table V. Plane parameters and Euler angles.

| Prismatic Lengths (mm) | | | Euler Angles (radians) | | |
|---|---|---|---|---|---|
| $P_X$ | = | 6.0161 | $\alpha$ | = | 0.7944 |
| $P_Y$ | = | 20.9114 | $\beta$ | = | 0.2754 |
| $P_Z$ | = | 17.7076 | $\gamma$ | = | 6.1246 |

In an effort to increase the space between the links, the threshold distance between the joints during the re-optimization was increased from 10 mm to 13 mm. The change to 13 mm was chosen as it would allow for increased link thickness to meet the strength requirements for the mechanism. The search was directed around the original solution by randomly generating a uniformly-distributed value around each parameter from the original solution. The new value was kept close to the seed value by setting the mean of the uniform distribution as the original value and setting the standard deviation of the distribution to be one tenth of the original value. This procedure found many potential candidates. The solution with the highest mechanical advantage also appeared to have the necessary joint space for manufacturing so it was selected. The profile for the mechanical advantage of the chosen solution is shown in Figure 18.

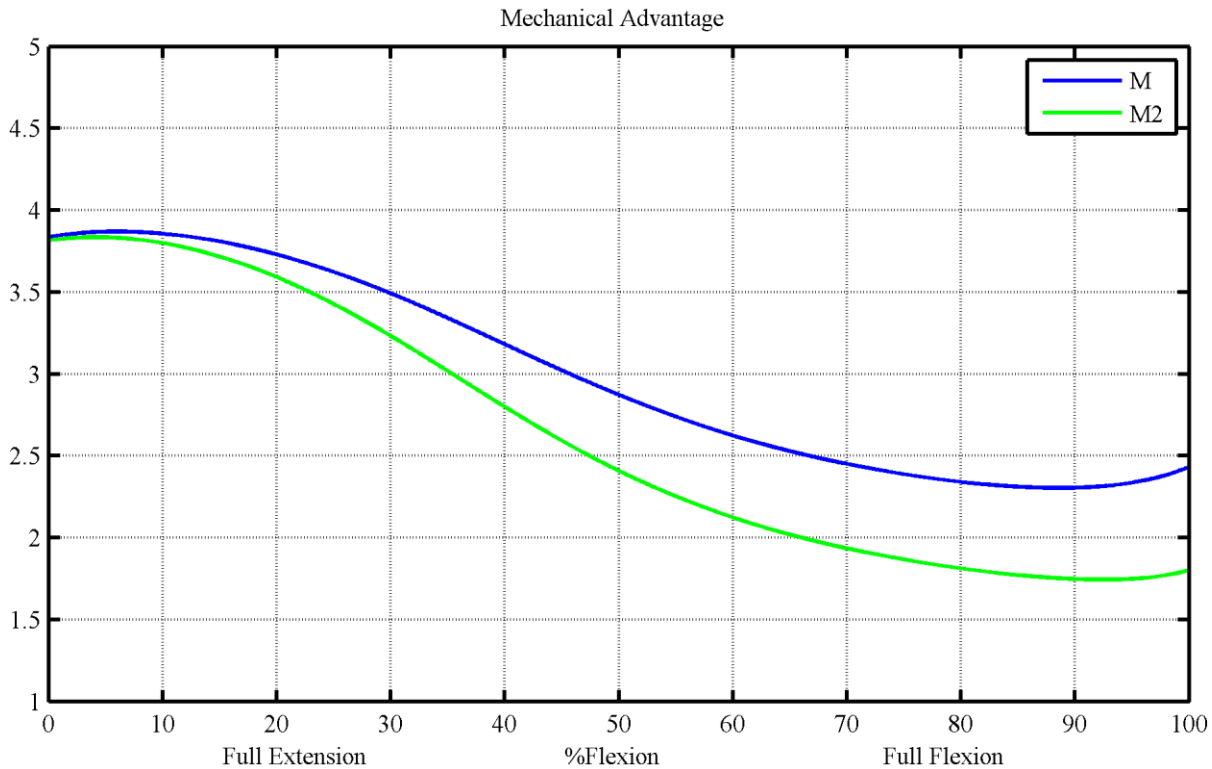


Figure 18. Mechanical advantage plot for the selected mechanism solution. The blue lines represent the mechanical advantage evaluated at node M on the end-effector. The green lines represent the mechanical advantage evaluated at node $M_2$ on the end-effector.

The mechanism found by this optimization procedure and selected for further design work has the parameters specified in Table VI. Table VII shows the parameters for the mechanism plane. Figure 12 shows the location of each parameter on the mechanism.

Table VI. Mechanism parameters and input angles for final solution.

| Structural Lengths (mm) | | | Structural Angles (radians) | | | Base Locations (mm) | | | Input Angles (radians) | | |
|---|---|---|---|---|---|---|---|---|---|---|---|
| $d_1$ | = | 46.6757 | $\alpha$ | = | 0.3489 | $G_x$ | = | 0.3660 | $\theta_{1,1}$ | = | 1.9792 |
| $d_2$ | = | 28.8466 | $\beta$ | = | 4.8025 | $G_y$ | = | 18.9935 | $\theta_{1,2}$ | = | 1.8464 |
| $d_3$ | = | 66.7359 | $\gamma_1$ | = | 1.0868 | $G_{1x}$ | = | 16.0884 | $\theta_{1,3}$ | = | 1.7280 |
| $d_4$ | = | 50.8125 | $\gamma_2$ | = | 0.6699 | $G_{1y}$ | = | 19.5264 | $\theta_{1,4}$ | = | 1.6201 |
| $d_5$ | = | 73.4167 | | | | | | | $\theta_{1,5}$ | = | 1.5236 |
| $d_6$ | = | 72.0971 | | | | | | | $\theta_{1,6}$ | = | 1.4345 |
| $d_7$ | = | 34.8915 | | | | | | | $\theta_{1,7}$ | = | 1.3491 |
| $d_8$ | = | 13.1845 | | | | | | | $\theta_{1,8}$ | = | 1.2622 |
| $d_9$ | = | 13.0000 | | | | | | | $\theta_{1,9}$ | = | 1.1725 |
| | | | | | | | | | $\theta_{1,10}$ | = | 1.0760 |
| | | | | | | | | | $\theta_{1,11}$ | = | 0.9614 |

Table VII. Plane parameters and Euler angles.

| Prismatic Lengths (mm) | | | Euler Angles (radians) | | |
|---|---|---|---|---|---|
| $P_X$ | = | 4.9102 | $\alpha$ | = | 0.6428 |
| $P_Y$ | = | 20.3295 | $\beta$ | = | 0.2681 |
| $P_Z$ | = | 15.9834 | $\gamma$ | = | 6.2723 |

Figure 19 shows both the geometry of the mechanism and how it matched the target points as it passed through all the configurations. The following plot shows a front view and a side view of the mechanism solution. Only the full extension configuration is shown in each plot with the mechanism. The trajectory of the mechanism is shown by the red dots which track the blue x's and o's that represent the target points corresponding to the thumb markers.

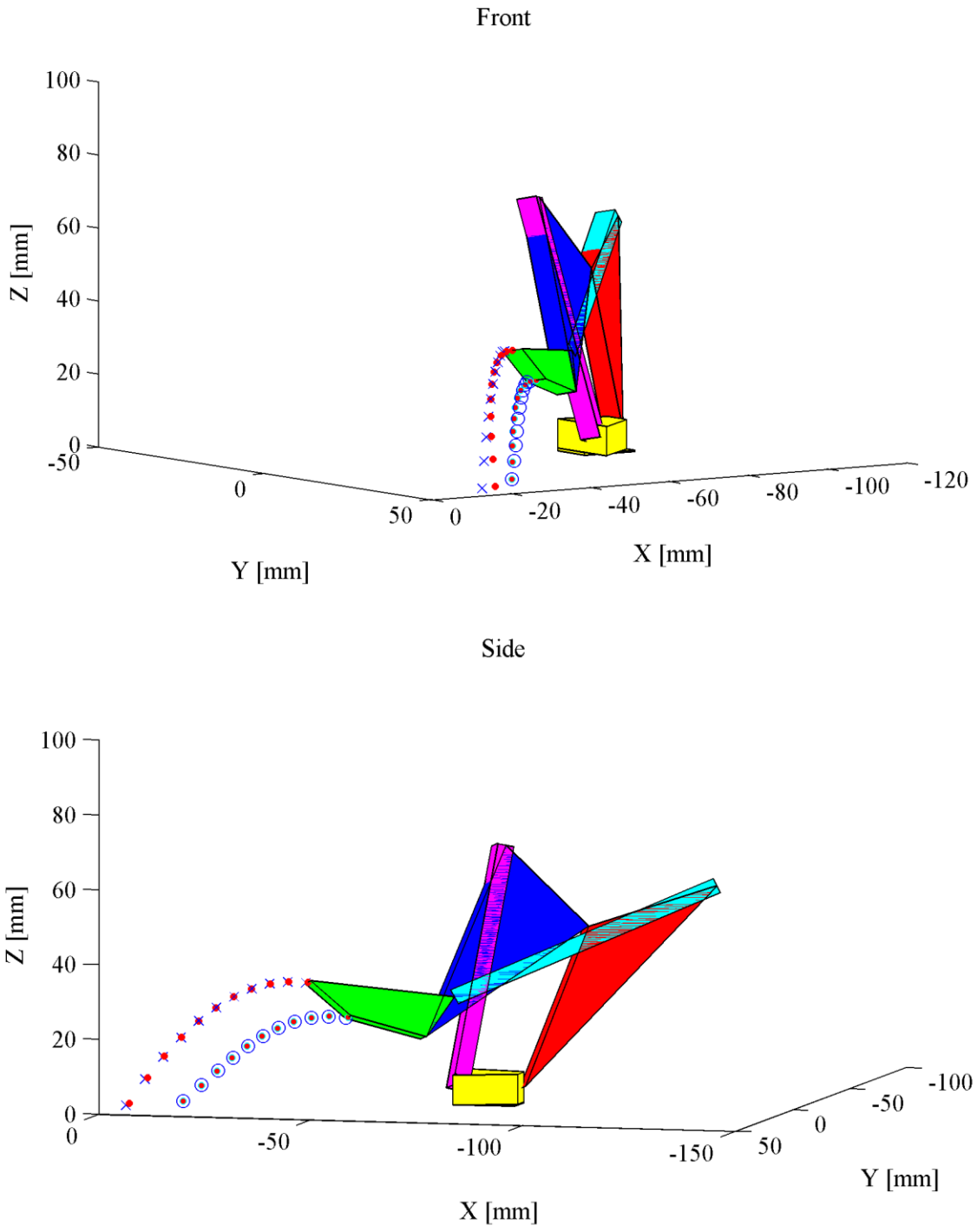


Figure 19. Front and side views of selected solution in full extension. The red dots trace the end effector path for all 11 configurations while the blue x's and o's trace the target path. All units are in millimeters.

The overall error for the mechanism was approximately 16.8 mm. When averaged over all 22 points, the error was 0.76 mm. Overall, the error for node M is lower with a mean error of 0.63 mm, while the mean error of $M_2$ is 0.89 mm. The error also varies less for node M, as it has a standard deviation of 0.41 mm, while node $M_2$ has a much larger deviation of 0.91 mm. These deviations are due to the out-of-plane motion of the thumb. This is expected since a planar mechanism is being fit to the non-planar motion of the thumb.

Figure 20 shows the overall error for each end-effector node for all 11 configurations along with the out-of-plane error. The errors for the lower nodes of the mechanism end-effector (M) are greatest in extension while the errors for the upper nodes of the mechanism end-effector ($M_2$) are greatest in flexion as the bar graph in Figure 20 goes from extension to flexion.

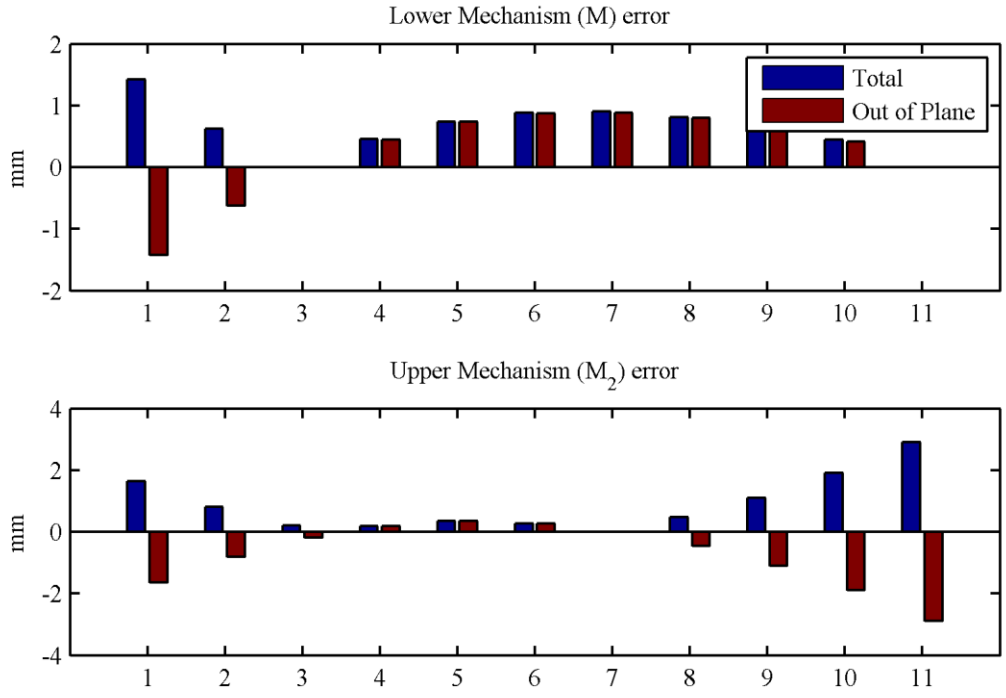


Figure 20. Absolute value of total error and signed out-of-plane error for upper and lower nodes of end-effector. The units for all values are millimeters.

Figure 21 shows two views that depict the out-of-plane nature of the error. The planar motion of the exoskeleton is represented by blue symbols, while the thumb target points are represented by green symbols. Figure 21 confirms most of the error occurs closer to full extension and flexion with the upper node $M_2$ (the blue square path) having most of the error.

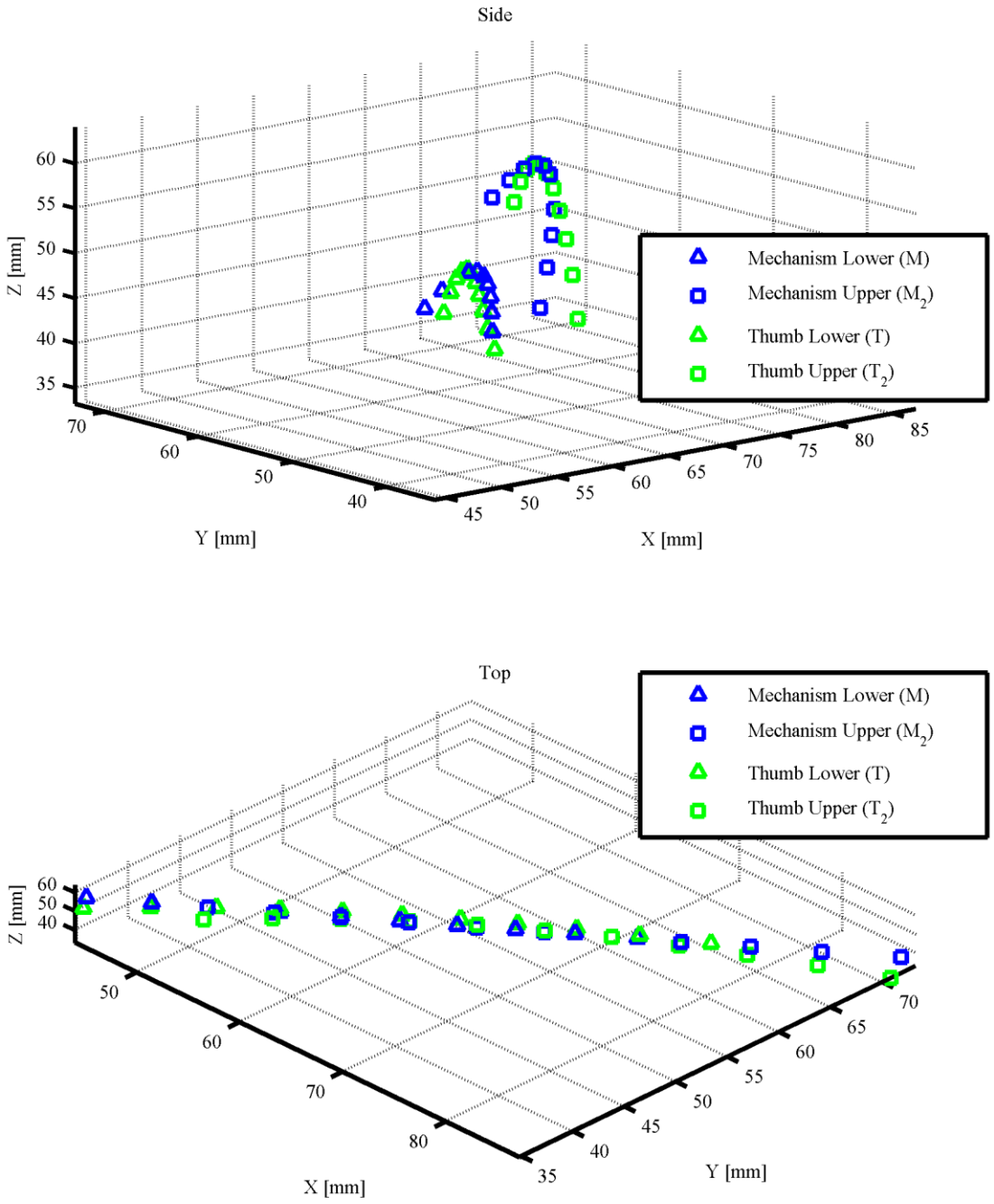


Figure 21. Location of the end-effector nodes in blue versus the thumb target points in green. The first subplot is taken from "behind" the hand. The second subplot is taken from "above" the hand.

# Chapter 5. Mechanical Design

## 5.1 Introduction

In order to demonstrate the viability of the mechanism design solution presented in the previous chapter and provide a baseline for future design work, an initial prototype was designed and manufactured. This chapter details the design and manufacturing process used to produce that prototype. Several factors guided this process. First, the prototype was meant to highlight any potential manufacturing issues which had not been addressed by the kinematic design process. The interface between the robot and the thumb and the robot and the actuator is also explored with this initial prototype. Another important consideration for the prototype is the attachment of the exoskeleton to the FINGER robot. Finally, the prototype provides a device for initial testing to inform the future development of the exoskeleton mechanism.

## 5.2 Design Objectives

While the optimization procedure screened many important manufacturing issues for the mechanism such as feasibility and the distance between joints, not every issue is practical to control with constraints and penalties or is even foreseeable. Even with the joint distance penalty, it is conceivable that the required geometry of a potential solution might lead to thin links that would fail during use. Another consideration for the design of the mechanism is the placement of mechanical stops that prevent over-extension or over-flexion in the case of failure of digital safeties. In addition, the driving link needs to be designed to attach to the actuator. This attachment node needs to be located in a manner that maximizes the mechanical advantage of the actuator, while not interfering with the function of the exoskeleton.

The location of the actuator is also a critical factor in the attachment of the thumb exoskeleton to FINGER. The actuator needs to be placed in a manner that maximizes the mechanical advantage, but not at the expense of significantly increasing the footprint of the FINGER robot or interfering with FINGER. The overall package of the exoskeleton and the actuator is ideally modular. This simplifies the addition of the thumb mechanism to the FINGER robot and could also lead to straightforward switching between right-handed and left-handed therapy. Of course, the module needs to remain out of the way of the patient both for safety reasons and to ease the process of donning the mechanism.

The interface between any rehabilitation robot and the limb that is being trained is critical. As such, the end-effector of the mechanism needs to fit the thumb, and ideally a wide range of thumbs, comfortably. Another factor that influences the usefulness of the robot-thumb interface is the ease of securing the thumb. This factor takes into account both the ease of placing the thumb in the cup and the method of securely fastening the thumb once it is placed in the cup. Comfort for the user is also important. Another aspect of the design of the interface between the thumb and the exoskeleton was the desire to make it easy to prototype.

The base of the exoskeleton needs to be designed in a manner that allows it to be attached to FINGER. This attachment needs to keep the thumb exoskeleton out of the way of both the patient and FINGER. Ideally the attachment uses some of the existing architecture of FINGER to minimize modifications to FINGER. Other desirable attributes for the attachment include the ability to switch between right- and left-handed therapy and adjustability to fit different patients.

## 5.3 Design Results

The exoskeleton mechanism that fulfilled these design objectives was designed in Solidworks. A prototype was created out of Polylactic Acid (PLA) using additive manufacturing (3D printing) on a Makerbot Replicator 2 to demonstrate the effectiveness of the design and provide a platform for initial tests. The prototype is shown in Figure 22.

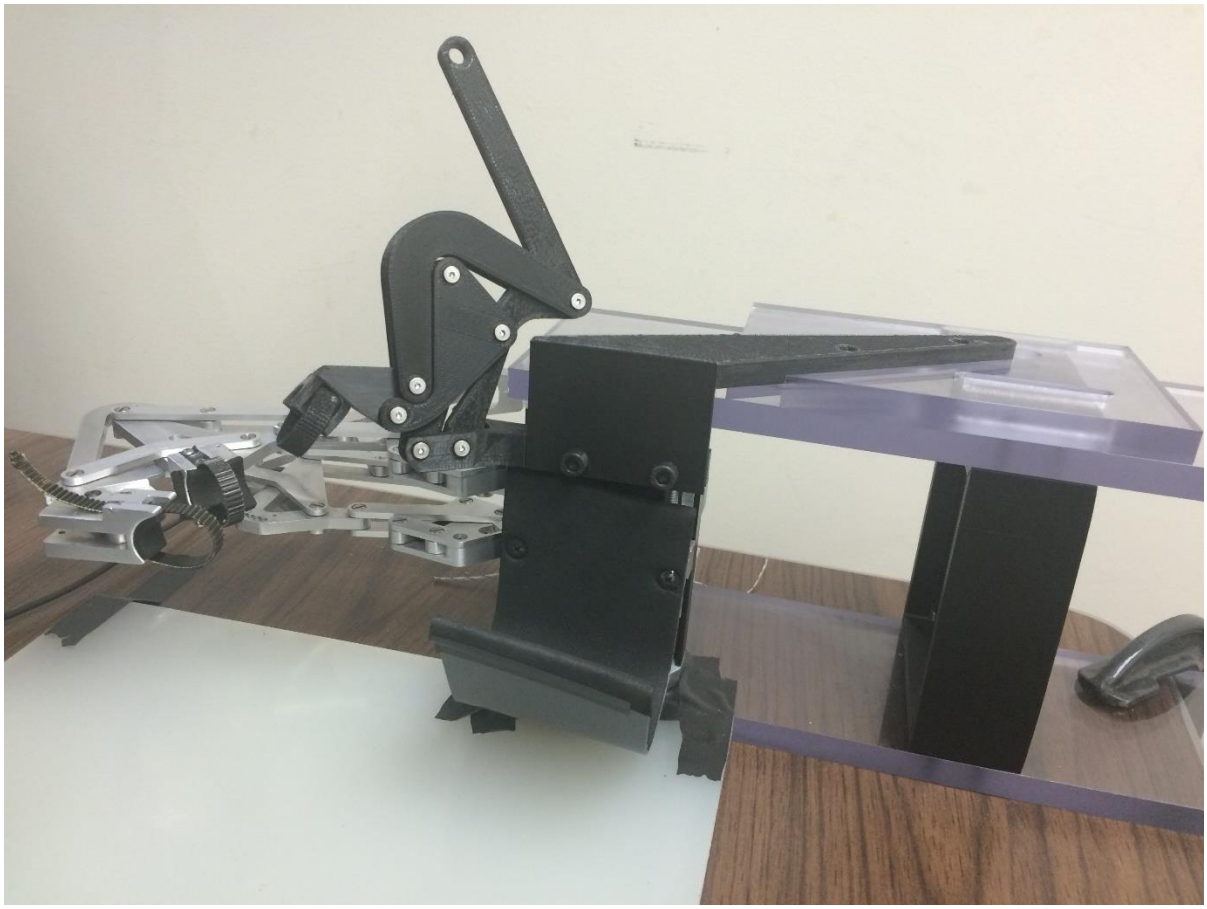

Figure 22. Full rapid prototyped mechanism with exoskeleton and adjustable base shown attached to a mockup of the housing for FINGER.

All the joints are designed to contain a quarter-inch bearing while having enough material around them to avoid failure. This follows the design which generally proved viable on FINGER [40]. The links are separated into inner and outer links. The inner links include the driving link and the end-effector to simplify the design of the attachment to both the thumb and actuator. The inner links are a quarter of an inch wide, while the outer links are an

eighth of an inch wide. The links are connected using eighth-inch shoulder bolts which run through two flanged quarter-inch bearings in the inner links. The shoulder bolts fasten into thin nuts inset in hexagonal cutouts on the backside of the outer links. This provides a more reliable fastening method than threading the plastic.

To prevent over-flexion, the base inner links were designed to contact each other at the end of flexion. Over-extension is prevented by contact between the middle base link and the end-effector link. The inner links have both hard stops due to their larger relative thickness compared with the outer links and to avoid excessive shear loading on the bearings. The extension hard stop is shown in Figure 23 and the flexion hard stop is shown in Figure 24 with the area of interest outlined by a red circle in each figure.

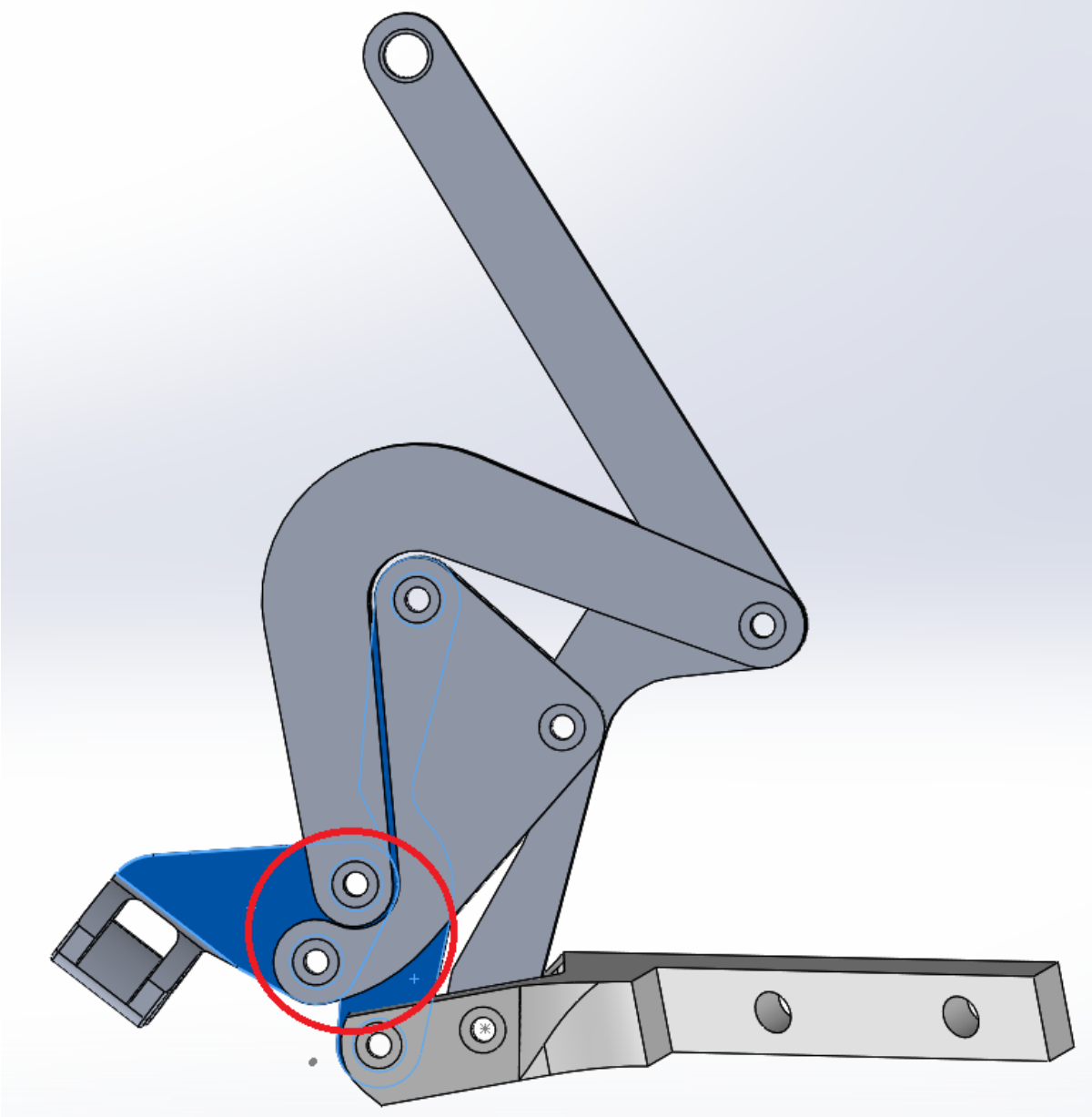

Figure 23. Mechanical contact in outer links preventing over-extension outlined in red.

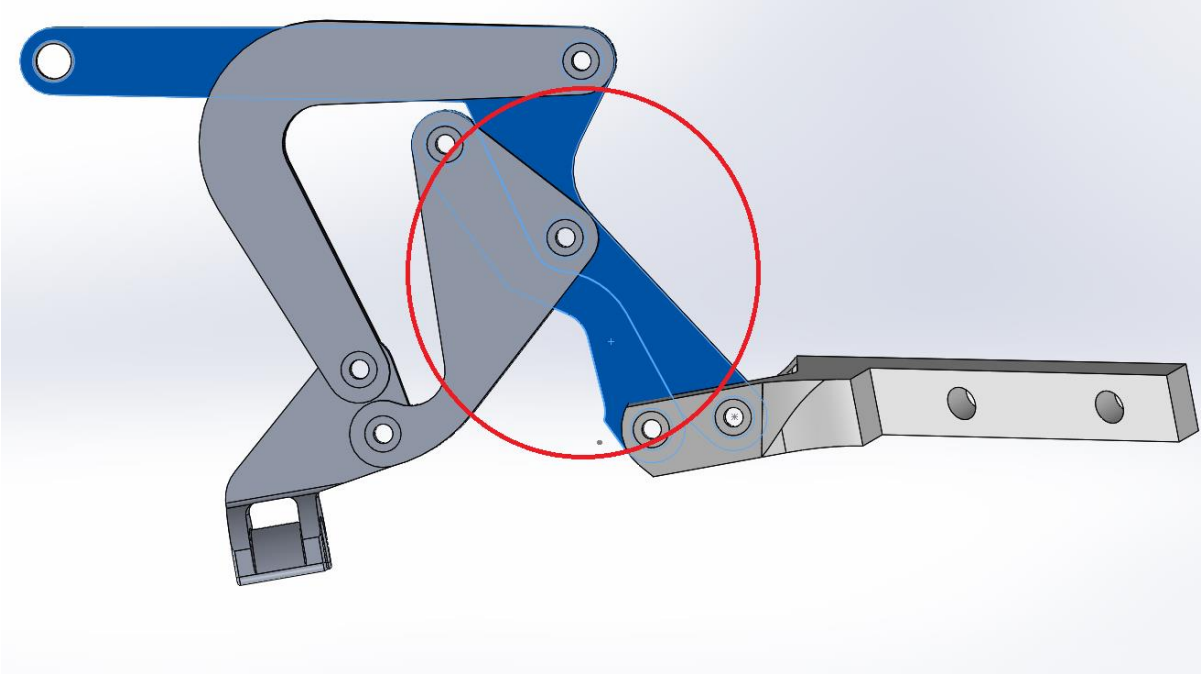

Figure 24. Mechanical contact in outer links preventing over-flexion outlined in red.

The design for the interface between the exoskeleton and the thumb is based on the finger cups used on FINGER. While FINGER has partial cups to provide directional support to the fingers during rehabilitation, the thumb interface is implemented as a complete semi-cylindrical cup to maximize contact with the back of the thumb. It is hoped that this design will enhance user comfort and the control of the thumb. While FINGER uses a ratcheting mechanism to hold the fingers in the cups, a simple hook and loop strap is used for this prototype due to its convenience. A close up view of the thumb cup is shown in Figure 25.

Figure 25. Close-up of interface between thumb and mechanism featuring a hook and loop strap.

The base for the thumb-exoskeleton mechanism is designed to be an add-on module that holds both the mechanism and the actuator, while it attaches to the existing architecture of FINGER. As presently designed, the module permits transverse and sagittal adjustment, but relies on the wrist height adjusting mechanism built into FINGER for vertical adjustment to accommodate various hand sizes. The three parts that make up the module are shown in Figure 26.

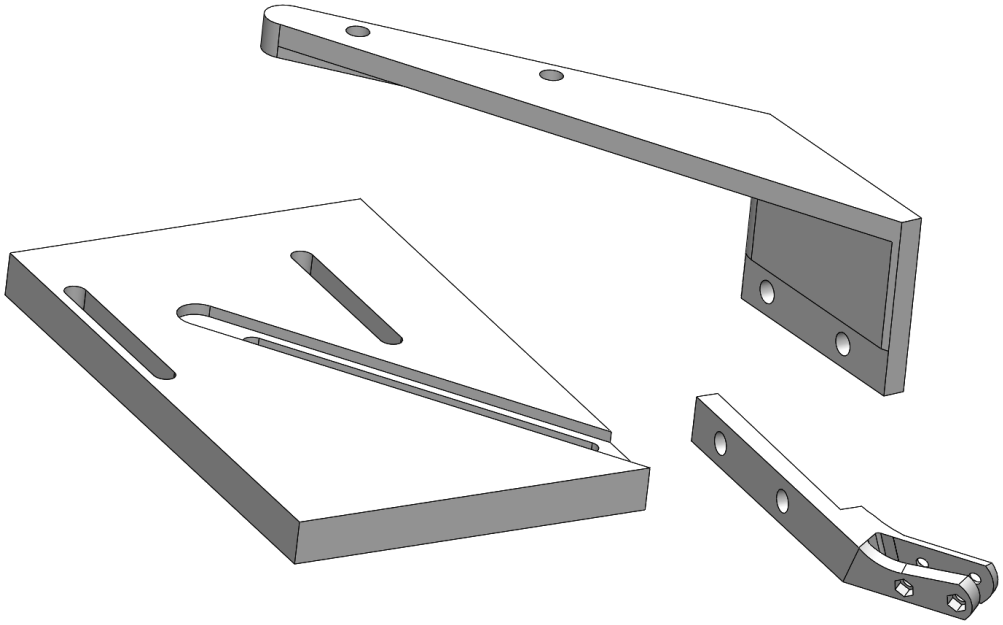

Figure 26. The thumb add-on module. From left to right: the base plate that attaches to the housing for FINGER, the intermediary component, the base for the thumb exoskeleton.

The first piece of the module is a plate that mounts to the top surface of the housing for FINGER. It is fastened to FINGER by bolts that attach to the actuator housing for FINGER. These bolts run through slots in the plate to permit sagittal adjustment. The plate also has a diagonal pair of slots on its top and bottom surface to allow both transverse and sagittal adjustment of the thumb exoskeleton. The angle of the slots is within the range of the angle between the exoskeleton plane and the housing for FINGER.

A second component bridges the gap between the plate and the base for the exoskeleton. This component contains a flange that runs in the diagonal slot of the plate. Two bolts run through this flange and are attached to nuts that are set in the slot on the base of the plate to fix the position of the intermediary component. A slight flange is part of the interface of the intermediary component with the base for the thumb exoskeleton to remove slop from that connection.

The base for the thumb exoskeleton is attached to the intermediary component by two bolts. The base for the exoskeleton is designed with minimal material beyond and below the location of the bolts for the base of the exoskeleton to avoid any potential contact with the thumb of a patient. A rendering of the full add-on attached to FINGER is shown in Figure 27.

Figure 27. Rendering of the thumb add-on attached to the housing for FINGER.

Another component of the mechanical design of the exoskeleton is the location of the actuator attachment. This is primarily constrained by two parameters. These parameters are the length of the moment arm determined by the original mechanical advantage analysis and the location of the actuator relative to the housing of FINGER. The goal of this aspect of the

design is to find an attachment point that will keep the actuator clear of the housing of FINGER, while enhancing the mechanical advantage of the mechanism.

The first step in finding the ideal location for the actuator attachment is to determine the effect of displacing the pivot point for the actuator above and below the horizontal line between the actuator attachment node in full flexion and full extension. The displacement of the pivot point is represented by Δy in Figure 28.

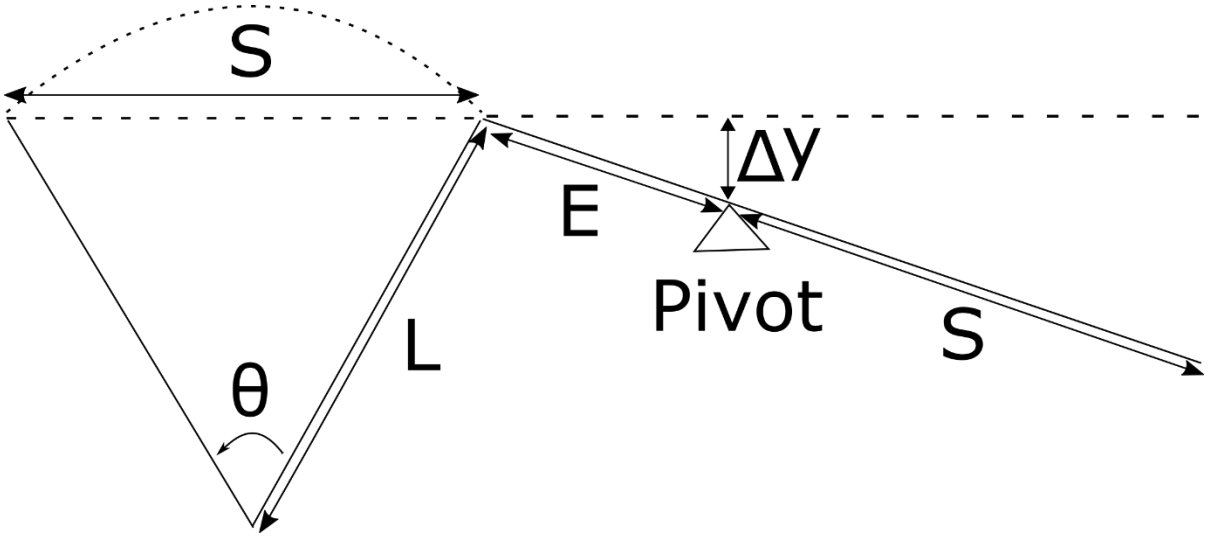


Figure 28. Figure describing calculation of mechanical advantage when the actuator pivot is offset. S is the stroke length. E is the distance from the actuator pivot to the attachment of the actuator to the exoskeleton. L is the lever arm length. The total transmission angle is θ. The offset is Δy.

A plot for the analysis of the offset mechanical advantage is shown in Figure 29. The plot shows both the mechanical advantage of the mechanism in extension as a solid blue line and the mean mechanical advantage for the mechanism over the complete motion of the exoskeleton as a dashed red line.

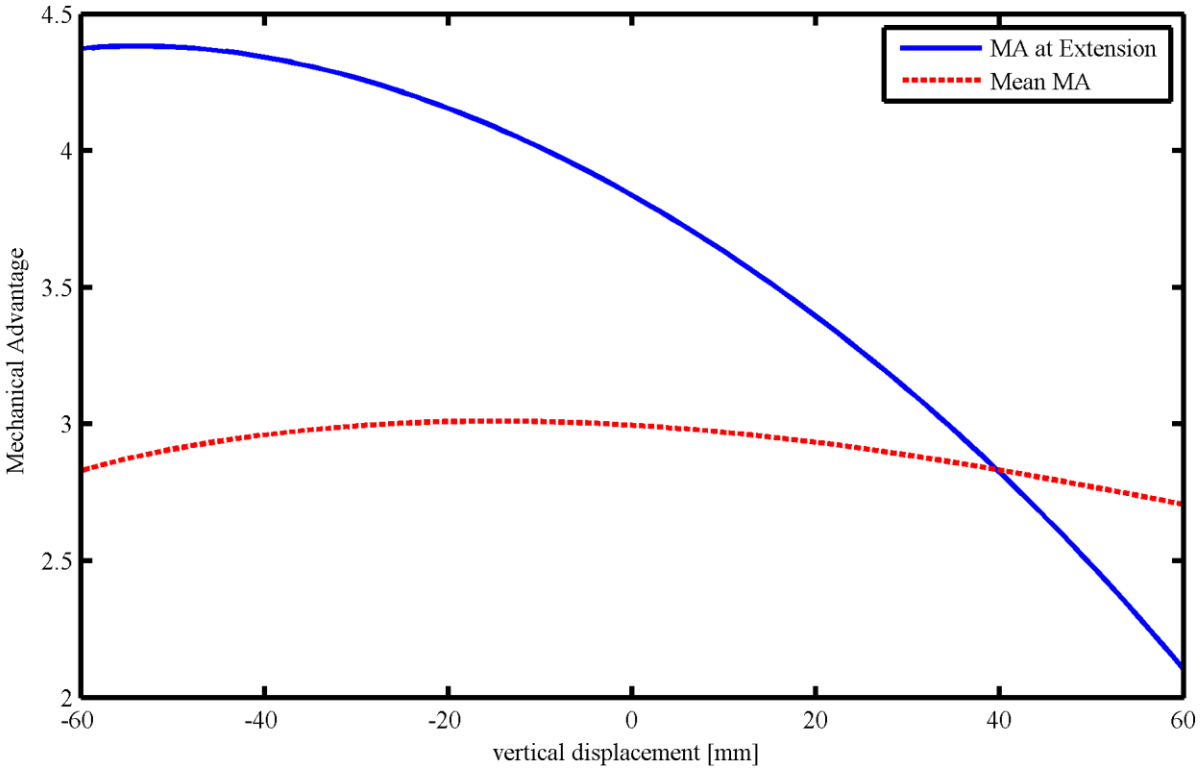


Figure 29. Change in mechanical advantage as pivot for actuator is changed vertically with the mechanical advantage in full extension for node M as a solid blue line and the mean mechanical advantage as a dashed red line. The vertical displacement is Δy in Figure 5.6.

From the plot above, peak mechanical advantage appears to occur when the pivot for the actuator is located about 55 mm below vertical, but the average mechanical advantage is largest at only 15 mm below vertical. Realistically, any location between 25 and 40 mm should be a reasonable compromise for a good overall mechanical advantage. Too large of a vertical displacement deteriorates the mechanical advantage in flexion, making the large peak extension value around 55 mm less desirable.

The position of the actuator with respect to the housing for FINGER makes selecting a large vertical displacement more challenging. By selecting a vertical displacement of 25 mm, the mechanical advantage is preserved. Furthermore, this value avoids geometrical issues with the actuator that would either require a re-design of the housing for FINGER or difficult geometry with the links of the exoskeleton. When compared with the non-offset

mechanical advantage in yellow and cyan, the plot in Figure 30 for the mechanism with a pivot displacement of -25 mm shows a significantly higher mechanical advantage in extension without too much loss in flexion.

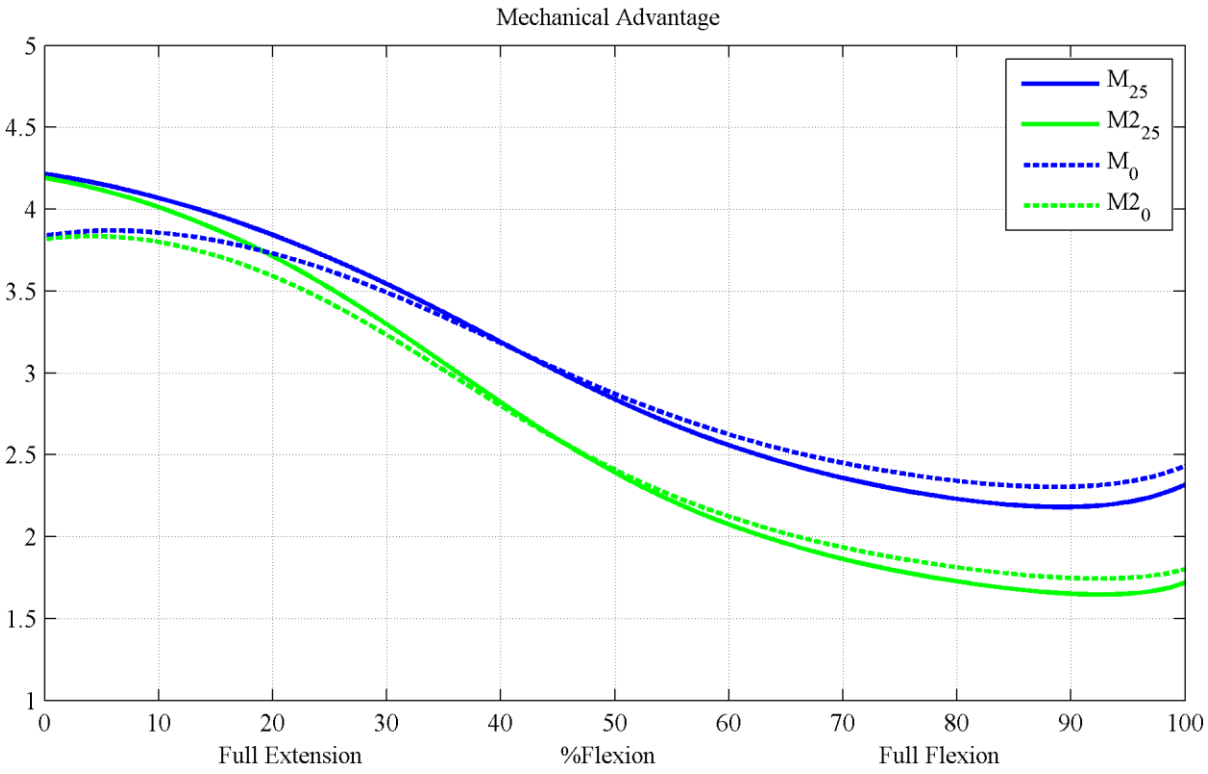


Figure 30. Mechanical advantage for mechanism with vertical displacement of actuator pivot point by 25 millimeters below horizontal in solid blue and green plotted against mechanical advantage with no displacement in dashed blue and green.

# Chapter 6. Conclusion

## 6.1 Summary of Work

This thesis describes the design and initial prototype of a thumb curling exoskeleton add-on device for the movement therapy robot FINGER. This process consisted of characterization of the thumb motion, mechanism synthesis, mechanism selection, and mechanism design and prototyping.

The thumb motion characterization process used a pair of cameras to track color-based markers on the thumb using Matlab. These tracks were processed together to form a three dimensional model of the motion of the middle phalanx of the thumb on the right hand. This characterization of the motion of the thumb, guided the synthesis of a mechanism that followed the trajectory and orientation of the middle phalanx of the thumb. The mechanism synthesis process used function minimization to find the dimensions and angles of a Watt I six-bar mechanism that closely follows the path of the thumb. Bounds on the optimized variables limited the size of the mechanism. Penalties added to the objective function kept the mechanism behind the thumb and kept the joints spaced apart.

Criteria such as manufacturability, geometric constraints, and mechanical advantage analysis regulated the selection of a particular mechanism from the many solutions produced during mechanism synthesis. Three solutions initially showed potential. The solution with the fewest geometric issues was used as a seed for a second round of mechanism synthesis to find the final solution.

Finally, a working prototype of the mechanism was designed along with a module to attach the mechanism to the housing for FINGER. This module provides sagittal and transverse adjustment to help fit the mechanism to various hand sizes. The design process

also includes mechanical advantage analysis to optimally position the pivot point for the actuator. The mechanism was constructed using an additive manufacturing process. Two components of the adjustable module were also constructed using three-dimensional printing. The base of the module which attaches to the housing for FINGER was machined on a CNC mill.

## 6.2 Discussion

Throughout the project decisions were made and assumptions were acted on that in hindsight may have slowed or tempered the success of this project. These problems were mostly present in two areas. These areas are the thumb path characterization and mechanism synthesis aspects of the project.

In the thumb path characterization, the coefficients of determination indicated that the curve fit worked well for each marker color, though it worked best for yellow, then blue, and was worst for red, which had an $R^2$ of 0.976. However, the thumb motion could have been more accurately tracked with a true stereovision system. A stereovision system would have eliminated the need for a raised marker so the thumb plane could have been tracked directly. This also would have kept all three markers closer to equidistant from the cameras throughout the motion of the thumb, reducing the potential for error due to distortion.

Furthermore, if the internal model of each camera had been determined, basic trigonometry along with the knowledge of the relative position of the markers to each other could have potentially enabled measurement of the position of the markers along the trajectory. This would have created a more precise set of tracking data than the composite of the top and side views did.

Despite the apparent accuracy of the curve fit, creating a true thumb model may have been more useful. This would have required tracking the proximal phalanx of the thumb along with the middle phalanx. By tracking both the proximal and middle phalanges of the thumb, a relationship could be established between the angles of the two phalanges. This would allow the movement of the thumb to be sampled using a set of input angles to the proximal phalanx instead of a linear spacing of input points as was done in this project. A thumb model could also be extended to work with a range of hand sizes and grasp motions.

For mechanism synthesis, the non-linear nature of the problem makes genetic algorithms a more natural fit than gradient based algorithms, which need a slope to follow to be most effective. In addition to replacing the gradient based algorithm with a heuristic process, the kinematics of the mechanism were defined in a manner that largely forced the mechanism to be classified as either feasible or infeasible. Again, problems without a defined gradient are difficult for optimizers to solve. A better method may have been to use loop equations and then minimize the separation between the joints in the loop along with minimizing the error between the end-effector and the thumb points.

One aspect of the mechanical design that warrants attention is the offset mechanical advantage. The analysis of the offset mechanical advantage showed only a small improvement in extension despite a significant offset. This low reward does not merit the sacrifice in design flexibility. Therefore, the offset should likely not be implemented in the final design. Instead the focus should be on aligning the actuator in a manner that is simple to use and adjust.

## 6. 3 Future Work

This prototype is meant to be a functional starting point for future design work. There are several areas in which this mechanism can be improved, and work still needs to be done to make the mechanism fully functional in a clinical research setting. Initially, it would be beneficial to do motion tracking for a variety of thumb sizes and grasp motions. The data collected could be used to create a general thumb model that could be used for modifying the mechanism to serve a variety of hand sizes, as FINGER does. It might also contribute to designs of the mechanism that could be modified to control different grasp tasks, enhancing the robot's range of use for therapy and research.

Additionally, the design of the mechanism could be modified to more closely track the out-of-plane motion of the thumb. This would eliminate the majority of the error between the thumb and the mechanism. Two modifications that would coordinate this mechanism's capabilities with FINGER's would be to add force sensing and design a method for easily switching the mechanism between modes for the right and left hand. Final work on the mechanism will involve manufacturing a therapy-grade device out of aluminum and designing the attachment of the actuator to the module and the exoskeleton in order to make the device fully operational. Another good modification to the prototype would be to incorporate FINGER's ratchet mechanism for the attachment of the robot's finger cups to the thumb.

# References

[1] Mozaffarian, Dariush; et al. on behalf of the American Heart Association Statistics Committee and Stroke Statistics Subcommittee, "Heart disease and stroke statistics-2015 update: a report from the American Heart Association," Circulation, 2015.

[2] G. Kwakkel, B. Kollen, J. van der Grond and A. Prevo, "Probability of regaining dexterity in the flaccid upper limb: Impact of severity of paresis and time since onset in accute stroke," *Stroke,* vol. 34, no. 9, pp. 2181-2186, 2003.

[3] K.-H. Kong, K. Chua and J. Lee, "Recovery of upper limb dexterity in patients more than 1 year after stroke: Frequency, clinical correlates and predictors," *NeuroRehabilitation,* vol. 28, no. 2, pp. 105-111, 2011.

[4] A.-K. Welmer, L. Holmqvist and D. Sommerfeld, "Limited fine hand use after stroke and its association with other disabilities," *Journal of Rehabilition Medicine,* vol. 40, no. 8, pp. 603-608, 2008.

[5] P. Langhome, J. Bernhardt and G. Kwakkel, "Stroke Rehabilitation," *The Lancet,* vol. 377, no. 9778, pp. 1693-1702, 2011.

[6] A. Turton and V. Pomeroy, "When should upper limb function be trianed after stroke? Evidence for and against early intervention," *Journal of NeuroRehabilitation,* vol. 17, no. 3, pp. 215-224, 2002.

[7] S. Maulden, J. Gassaway, S. Horn, R. Smout and G. DeJong, "Timing of Initiation of Rehabilitation After Stroke," *Archives of Physical Medicine and Rehabilitation,* vol. 86, no. Supplemental 2, pp. S34-S40, 2005.

[8] C. Burgar, P. Lum, P. Shor and M. Van der Loos, "Development of robots for rehabilitation therapy: The Palo Alto VA/Stanford experience," *Journal of Rehabilitation Research and Development,* vol. 37, no. 6, pp. 663-673, 2000.

[9] P. Langhorne, F. Coupar and A. Pollock, "Motor recovery after stroke: a systematic review," *Lancet Neurology,* vol. 8, no. 8, pp. 741-754, 2009.

[10] J. Veerbeek, E. van Wegen, R. van Peppen, P. van der Wees, E. Hendriks, M. Rietberg and G. Kwakkel, "What is the evidence for physical therapy poststroke? A systematic review and meta-analysis," *PLoS ONE,* vol. 9, no. 2, p. e87987, 2014.

[11] S. Wolf, P. Thompson, C. Winstein, J. Miller, S. Blanton, D. Nichols-Larsen, D. Morris, G. Uswatte, E. Taub, K. Light and L. Sawaki, "The EXCITE Stroke Trial:

Comparing early and delayed Constraint-Induced Movement Therapy," *Stroke,* vol. 41, no. 10, pp. 2309-2315, 2010.

[12] S. Page, P. Levine and A. Leonard, "Mental practice in chronic stroke: results of a randomized, placebo-controlled trial," *Stroke,* vol. 38, no. 4, pp. 1293-1297, 2007.

[13] J. Cauraugh, K. Light, S. Kim, M. Thigpen and A. Behrman, "Chronic motor dysfunction after stroke: Recovering wrist and finger extension by electromyograhy-triggered neuromuscular stimulation," *Stroke,* vol. 31, no. 6, pp. 1360-1364, 2000.

[14] J. Chae, F. Bethoux, T. Bohinc, L. Dobos, T. Davis and A. Friedl, "Neuromuscular stimulation for upper extremity motor and functional recovery in acute hemiplegia," *Stroke,* vol. 29, no. 5, pp. 975-979, 1998.

[15] H. Woodford and C. Price, "Electromyographic biofeedback for the recovery of motor function after stroke," *Stroke,* vol. 38, no. 6, pp. 1999-2000, 2007.

[16] N. Norouzi-Gheidari, P. Archambault and J. Fung, "Effects of robot-assisted therapy on stroke rehabilitation in upper limbs: Systematic review and meta-analysis of the literature," *Journal of Rehabilitation Research and Development,* vol. 49, no. 4, pp. 479-496, 2012.

[17] J. Mehrholz, A. Hadrich, J. Kugler and M. Pohl, "Electromechanical and robot-assisted arm training after stroke (Updated Review)," *Stroke,* vol. 43, no. 12, p. e172+, 2012.

[18] G. Prange, M. Jannink, C. Groothuis-Oudshoorn, H. Hermens and M. Ijzerman, "Systematic review of the effect of robot-aided therapy on recovery of hemiparetic arm after stroke," *Journal of Rehabilitation Research and Development,* vol. 43, no. 2, pp. 171-184, 2006.

[19] A. Lo and e. al., "Robot-assisted therapy for long-term upper-limb impairment after stroke," *New England Journal of Medicine,* vol. 362, no. 17, pp. 72-83, 2010.

[20] K. Arya, S. Pandian, R. Verma and R. Garg, "Movement therapy induced neural reorganization and motor recovery in stroke: A review," *Journal of Bodywork and Movement Therapies,* vol. 15, no. 4, pp. 528-537, 2011.

[21] D. Reinkensmeyer, J. Emken and S. Cramer, "Robotics, motor learning, and neurologic recovery," *Annual Review of Biomedical Engineering,* vol. 6, pp. 497-525, 2004.

[22] R. Colombo, F. Pisano, A. Mazzone, C. Delconte, S. Micera, M. Carrozza, P. Dario and G. Minuco, "Design strategies to improve patient motivation during robot-aided rehabilitation," *Journal of NeuroEngineering and Rehabilitation,* vol. 4, no. 3, 2007.

[23] L. Kahn, P. Lum, W. Rymer and D. Reinkensmeyer, "Robot-assisted movment training for the stroke-impaired arm: Does it matter what the robot does?," *Journal of Rehabilitation Research and Development,* vol. 43, no. 5, pp. 619-630, 2006.

[24] P. Lum, D. Reinkensmeyer, R. Mahoney, W. Rymer and C. Burgar, "Robotic devices for movement therapy after stroke: Current status and challenges to clinical acceptance," *Topics in Stroke Rehabilitation,* vol. 8, no. 4, pp. 40-53, 2002.

[25] P. Maciejasz, J. Eschweiler, K. Gerlach-Hahn, A. Jansen-Troy and S. Leonhardt, "A survey on robotic devices for upper limb rehabilitation," *Journal of Neuroengineering and Rehabilitation,* vol. 11, no. 3, 2014.

[26] L. Connelly, M. Stoykov, Y. Jia, M. Toro, R. Kenyon and D. Kamper, "Use of a pneumatic glove for hand rehabilitation following stroke," in *31st Annual International Conference of the IEEE EMBS* , Minneapolis, Minnesota, 2009.

[27] L. Dovat, O. Lambercy, R. Gassert, T. Maeder, T. Milner, T. Leong and E. Burdet, "HandCARE: A cable-actuated rehabilitation system to train hand function after stroke," *IEEE Transactions on Neural Systems and Rehabilitation Engineering,* vol. 16, no. 6, pp. 582-591, 2008.

[28] M. Chen, S. Ho, H. Zhou, P. Pang, X. Hu, D. Ng and K. Tong, "Interactive rehabilitation robot for hand function training," in *2009 IEEE International Conference on Rehabilitation Robotics,* Kyoto, Japan, 2009.

[29] C. Schabowsky, S. Godfrey, R. Holley and P. Lum, "Development and pilot testing of HEXORR: Hand EXOskeleton rehabilitation robot," *Journal of Neuroengineering and rehabilitation,* vol. 7, no. 36, 2010.

[30] R. Sanchez, E. Wolbrecht, R. Smith, J. Liu, S. Rao, S. Cramer, J. Bobrow and D. Reinkensmeyer, "A pneumatic robot for re-training arm movement after stroke: Rationale and mechanical design," in *International Conference on Rehabilitation Robotics*, Chicago, 2005.

[31] C. Takahashi, L. Der-Yeghiaian, V. Le and S. Cramer, "A robotic device for hand motor therapy after stroke," in *International Conference on Rehabiliation Robotics*, Chicago, 2005.

[32] E. Koeneman, R. Schultz, S. Wolf, D. Herring and J. Koeneman, "A pneumatic muscle hand therapy device," in *International Conference of the IEEE EMBS*, San Francisco, 2004.

[33] H. Taheri, J. Rowe, D. Gardner, V. Chan, K. Gray, C. Bower, D. Reinkensmeyer and E. Wolbrecht, "Design and preliminary evaluation of the FINGER rehabilitation robot:

controlling challenge and quantifying finger individuation during musical computer game play," *Journal of Neuroengineering and Rehabilitation,* vol. 11:10, 2014.

[34] Y. Yihun, R. Miklos, A. Perez-Garcia, D. Reinkensmeyer, K. Denney and E. Wolbrecht, "Single degree-of-freedom exoskeleton mechanism design for thumb rehabilitation," in *34th Annual International Conference of the IEEE EMBS,* San Diego, California, 2012.

[35] O. Lambercy, D. Schroeder, S. Zwicker and R. Gassert, "Design of a thumb exoskeleton for hand rehabilitation," in *Proceedings of the International Convention on Rehabilitation Engineering and Assistive Technology*, Seoul, 2013.

[36] B. Heisele and W. Ritter, "Obstacle dectection based on color blob flow," in *Proceedings of the Intelligent Vehicles 1995 Symposium*, Detroit, MI, 1995.

[37] B. Heisele, U. Kressel and W. Ritter, "Tracking non-rigid, moving objects based on color cluster flow," in *1997 IEEE Computer Society Conference on Computer Vision and Pattern Recognition*, 1997.

[38] T. Feix, R. Pawlik, H. Schmiedmayer, J. Romero and D. Kragic, "A comprehensive grasp taxonomy," in *Robotics, Science, and Systems: Workshop on Understanding the Human Hand for Advancing Robotic Manipulation*, June 2009.

[39] D. Sands, A. Perez-Garcia, J. McCormack and E. Wolbrecht, "Design method for a reconfigurable mechanism for finger rehabilitation," in *IASTED Technology Conferences*, Cambridge, 2010.

[40] D. Gardner, *Exoskeleton Robot for Finger Rehabilitation: Mechanism Synthesis, Design, and Manufacture,* M.S. thesis, Dept. Mech. Eng., University of Idaho, Moscow, ID, 2012.

[41] R. Sabini, M. Dijkers and P. Raghavan, "Stroke survivors talk while doing: Development of a therapeutic framework for continued rehabilitation of hand function post stroke," *Journal of Hand Therapy,* vol. 26, no. 2, pp. 124-131, 2013.

[42] E. Wolbrecht, D. Reinkensmeyer and A. Perez-Garcia, "Single degree-of-freedom exoskeleton mechanism design for finger rehabilitation," in *2011 IEEE International Conference on Rehabilitation Robotics (ICORR)*, 2011.

[43] D. Kamper, H. Fischer, M. Conrad, J. Towles, W. Rymer and K. Triandafilou, "Finger-thumb coupling contributes to exagerated thumb flexion in stroke survivors," *Journal of Neurophysiology,* vol. 111, no. 12, pp. 2665-2674, 15 June 2014.

# Appendix A. Target Points for Mechanism Synthesis

This table contains the pairs of target points for mechanism synthesis. These 11 pairs of points were sampled from the thumb path characterization results. All units are in millimeters.

| **T** | | | **$T_2$** | | |
|---|---|---|---|---|---|
| **x** | **y** | **z** | **x** | **y** | **z** |
| -50.1457 | 19.8441 | 23.8259 | -41.403 | 22.7307 | 33.3084 |
| -46.8592 | 23.0552 | 24.4624 | -38.0609 | 26.0639 | 33.8551 |
| -43.6611 | 26.2167 | 24.3967 | -34.716 | 29.3811 | 33.5975 |
| -40.5606 | 29.3175 | 23.6524 | -31.3744 | 32.6755 | 32.5418 |
| -37.5681 | 32.3459 | 22.2682 | -28.043 | 35.9401 | 30.6966 |
| -34.6906 | 35.2946 | 20.304 | -24.7279 | 39.1716 | 28.0757 |
| -31.9198 | 38.1717 | 17.8443 | -21.4303 | 42.3774 | 24.6976 |
| -29.2087 | 41.0188 | 14.9901 | -18.137 | 45.5888 | 20.5775 |
| -26.4394 | 43.9308 | 11.8161 | -14.8107 | 48.868 | 15.6997 |
| -23.4138 | 47.0437 | 8.2824 | -11.4005 | 52.2862 | 9.98 |
| -19.93 | 50.4645 | 4.1612 | -7.8962 | 55.8582 | 3.2785 |

# Appendix B. Six-Bar Kinematics

These equations are a completion of Equation (5) and use the variables shown in Figure 12 to describe the motion of each node in Figure 12 using forward kinematics and constraints.

$$\angle GG_1 = atan2(G_{1y} - G_y\,, G_{1x} - G_x)$$

$$\angle AG_1 = atan2(G_{1y} - A_y\,, G_{1x} - A_x)$$

$$\overline{AG_1} = \sqrt{\overline{\left(A_y - G_{1y}\right)^2 + (A_x - G_{1x})^2}}$$

$$\angle G_1AB = \operatorname{acos}\left(\frac{\overline{AG_1}^2 + d_2^2 - d_3^2}{2\overline{AG_1}d_2}\right)$$

$$\angle DC = atan2(C_y - D_y\,, C_x - D_x)$$

$$\overline{DC} = \sqrt{\overline{\left(D_y - C_y\right)^2 + (D_x - C_x)^2}}$$

$$\angle EDC = \operatorname{acos}\left(\frac{\overline{DC}^2 + d_6^2 - d_9^2}{2\overline{DC}d_6}\right)$$

$$\angle EC = atan2(C_y - E_y\,, C_x - E_x)$$

$$\angle M_2E = atan2(E_y - M_{2y}\,, E_x - M_{2x})$$

$$\boldsymbol{A} = \boldsymbol{G} + d_1\begin{pmatrix}sin\\cos\end{pmatrix}(\angle GG_1 + \theta_1)$$

$$\boldsymbol{B} = \boldsymbol{A} + d_2\begin{pmatrix}sin\\cos\end{pmatrix}(\angle G_1AB - \angle AG_1)$$

$$\boldsymbol{C} = \boldsymbol{A} + d_4\begin{pmatrix}sin\\cos\end{pmatrix}(\angle G_1AB + \angle AG_1 + \beta)$$

$$\boldsymbol{D} = \boldsymbol{G} + d_5 \begin{pmatrix} sin \\ cos \end{pmatrix} (\angle GG_1 + \theta_1 + \alpha)$$

$$\boldsymbol{E} = \boldsymbol{D} + d_6 \begin{pmatrix} sin \\ cos \end{pmatrix} (\angle DC + \angle EDC)$$

$$\boldsymbol{M} = \boldsymbol{M_2} + d_8 \begin{pmatrix} sin \\ cos \end{pmatrix} (\angle M_2E + \gamma_2)$$

$$\boldsymbol{M_2} = \boldsymbol{E} + d_7 \begin{pmatrix} sin \\ cos \end{pmatrix} (\angle EC - \gamma_2)$$